

Nonparametric Measure-Transportation-Based Methods for Directional Data

Hallin M.^{1*} — Liu H.² — Verdebout T.^{1†}

¹ECARES and Département de Mathématique, Université libre de Bruxelles

²International Institute of Finance, School of Management, University of Science and Technology of China

Correspondence

Marc Hallin, Université libre de Bruxelles, ECARES and Département de Mathématique, Brussels, B-1050, Belgium
Email: mhallin@ulb.ac.be

Funding information

Thomas Verdebout's research is supported by an ARC grant of the ULB and the Communauté Française de Belgique, a Projet de Recherche (PDR) grant of the FNRS, and the Fonds Thelam of the Fondation Roi Baudouin.

This paper proposes various nonparametric tools based on measure transportation for directional data. We use optimal transports to define new notions of distribution and quantile functions on the hypersphere, with meaningful quantile contours and regions yielding closed-form formulas under the classical assumption of rotational symmetry. The empirical versions of our distribution functions enjoy the expected Glivenko-Cantelli property of traditional distribution functions. They provide fully distribution-free concepts of ranks and signs and define data-driven systems of (curvilinear) parallels and (hyper)meridians. Based on this, we also construct a universally consistent test of uniformity which, in simulations, outperforms the “projected” Cramér-von Mises, Anderson-Darling, and Rothman procedures recently proposed in the literature. We also propose fully distribution-free rank- and sign-based tests for directional MANOVA. Two real-data examples involving the analysis of sunspots and proteins structures conclude the paper.

KEYWORDS

directional statistics, directional quantiles, ranks, signs, optimal transport, directional MANOVA

1 — INTRODUCTION

Directional data analysis is dealing with random directions—taking values on circles and (hyper)spheres or, more generally, on manifolds. Directional data can be found in a variety of fields, including astronomy ([Marinucci et al., 2008](#);

Marinucci and Peccati, 2011), *environmetrics* (García-Portugués et al., 2014; Ameijeiras-Alonso et al., 2018; Kume and Sei, 2018), biology and medicine (Dryden, 2005; Hamelryck et al., 2006; Dortet-Bernadet and Wicker, 2008), to cite only a few. Directions generally are represented as points on the unit hypersphere $S^{d-1} := \{\mathbf{x} \in \mathbb{R}^d : \|\mathbf{x}\|^2 := \mathbf{x}^\top \mathbf{x} = 1\}$ in \mathbb{R}^d . The special nature of their sample spaces gives directional statistics a specific flavor. The models of interest are of the standard statistical types (one-sample and multi-sample location, analysis of variance, regression, etc.) and inference is carried out according to the usual principles, but their implementation takes special forms and requires distinctive techniques. A comprehensive exposition of the theoretical background and inference methods for circular and spherical data can be found in Mardia and Jupp (1999) or Watamori and Jupp (2005). More recent advances are presented in Ley and Verdebout (2017, 2018); Rao and SenGupta (2001) provide a detailed account of distributions on the circle while statistical tools for data on more general spaces are studied in Chikuse (2003).

The most popular parametric model in directional statistics, which can be traced back to the first decades of the 20th century, is the von Mises-Fisher model, characterized by the family of von Mises distributions, with densities (with respect to the classical surface area measure on S^{d-1}) of the form

$$\mathbf{z} \in S^{d-1} \mapsto c_\kappa \exp(\kappa \mathbf{z}^\top \boldsymbol{\theta}), \quad (1.1)$$

where $\boldsymbol{\theta} \in S^{d-1}$ plays the role of a location parameter, $\kappa \in \mathbb{R}^+$, which drives the probability mass in the vicinity of $\boldsymbol{\theta}$, is the so-called *concentration parameter*, and c_κ is a normalizing constant. The von Mises distribution is often seen as the “directional Gaussian” distribution due to the fact that the maximum likelihood estimator of $\boldsymbol{\theta}$ is the normalized sample average.

The von Mises distributions belong to the more general class of rotationally symmetric distributions, which contains all distributions with densities (still with respect to the surface area measure on S^{d-1}) of the form

$$\mathbf{z} \in S^{d-1} \mapsto c_f f(\mathbf{z}^\top \boldsymbol{\theta}), \quad (1.2)$$

where $\boldsymbol{\theta} \in S^{d-1}$, f is some positive *angular function*, and c_f is a norming constant. The projection $(\mathbf{I}_p - \boldsymbol{\theta}\boldsymbol{\theta}^\top)\mathbf{Z}$ of a rotationally symmetric random vector \mathbf{Z} has a spherical distribution in the tangent space (to S^{d-1}) at $\boldsymbol{\theta}$. Inference for the parameters of rotationally symmetric distributions has recently been considered in Christie (2015), Kanika et al. (2015), and Paidaveine and Verdebout (2020a,b). Extensions of rotational symmetry yielding, after projection in the tangent space (to S^{d-1}) at $\boldsymbol{\theta}$, distributions with elliptic contours have been proposed in Kent (1982), Scaely and Wood (2019) and García-Portugués et al. (2020); see also Kume et al. (2013), Kume and Sei (2018) and Kent et al. (2018). Rank-based methods for directional data have been proposed in Ley et al. (2013, 2017) and Verdebout (2017). While the concepts of ranks considered there enjoy several attractive features, their distribution-freeness, hence also their applicability is limited to rotational symmetry. Based on sample projections onto the mean direction, the quantiles studied in Ley et al. (2014) are canonical for rotationally symmetric distributions on S^{d-1} but fail to be informative for general distributions on S^{d-1} . The assumptions of rotational symmetry and their “elliptical extensions” are pervasive in the literature on directional data; they can be compared, in this respect, to the assumptions of spherical and elliptical symmetry in traditional multivariate analysis. Just as the latter, they drastically simplify the mathematical structure of inference problems but also very severely restrict their validity: in most applications, rotational symmetry, indeed, is extremely unlikely to hold.

The situation in the directional context, thus, is quite comparable to the situation in the general multivariate context: the absence of a canonical ordering, at first sight, precludes the canonical definition of essential order-related statistical tools as ranks, signs, and quantiles unless one is ready to make a very strong assumption of rotational symmetry (or its “elliptical extensions”) in the directional case, of spherical or elliptical symmetry in the general multivariate

case. Based on measure transportation ideas and novel concepts of multivariate distribution and quantile functions in \mathbb{R}^d , new non- and semi-parametric methods have been proposed very recently in Chernozhukov et al. (2017) and Hallin et al. (2021a), which have demonstrated their efficiency in a variety of multivariate inference problems: see Deb et al. (2021), Hallin et al. (2021b), Ghosal and Sen (2022), Hallin et al. (2022a,b,c), Shi et al. (2022a,b), del Barrio et al. (2022), Deb and Sen (2022). Torous et al. (2022) use optimal transport to perform causal inference, while machine learning methods based on optimal transport have been proposed, e.g., in Kolouri et al. (2017). See Hallin (2022) for a nontechnical survey.

All the above references are dealing with observations and transports in \mathbb{R}^d . In the present paper, we consider transports on hyperspheres providing various nonparametric tools for directional data and show that they can be seen as canonical transformations in the sense of Jupp and Kume (2020). We first propose a new concept of *directional distribution function* $\mathbf{F} : S^{d-1} \rightarrow S^{d-1}$ based on an optimal transport from the distribution under study to the uniform over S^{d-1} . The corresponding empirical distribution function $\mathbf{F}^{(n)}$ provides several efficient tools for non- and semi-parametric inference, data analysis, and graphical representation problems. In particular, it defines fully distribution-free ranks and signs allowing for rank-based inference. The corresponding empirical quantile contours constitute powerful data-analytic tools and yield highly informative graphic representations. Empirical distribution functions also naturally bring in goodness-of-fit and MANOVA tests: as examples, we propose (i) a Cramér-Von Mises-type test of uniformity on S^{d-1} based on $\mathbf{F}^{(n)}$ —we show that it is *universally* consistent and outperforms its recent competitors—and (ii) distribution-free MANOVA procedures.

The paper is organized as follows. In Section 2, we provide the relevant mathematical notions and briefly discuss the concept of measure transportation on Riemannian manifolds and hyperspheres. We define the population versions \mathbf{F} and \mathbf{Q} of our directional distribution and quantile functions in Section 3, then derive their explicit forms in the rotationally symmetric case. In Section 4, we introduce the empirical version $\mathbf{F}^{(n)}$ of \mathbf{F} and establish its Glivenko-Cantelli asymptotic behavior. We also introduce the resulting ranks and signs and discuss their distributional and equivariance properties. Section 4.4 illustrates the construction of empirical quantile contours in simulated data. In Section 5, based on $\mathbf{F}^{(n)}$, we construct Cramér-Von Mises-type tests for goodness-of-fit problems, establish their universal consistency against fixed alternatives, and compare their performance with that of several recent competitors. In Section 6, we propose distribution-free MANOVA testing procedures. Real-data applications are presented in Section 7 where we implement our MANOVA procedure on sunspots data and illustrate our novel concept of directional quantiles in an analysis of proteins structures.

2 — MEASURE TRANSPORTATION ON RIEMANNIAN MANIFOLDS

Throughout the paper, we denote by $d(\mathbf{y}, \mathbf{z}) := \cos^{-1}(\mathbf{y}^\top \mathbf{z})$ the geodesic distance and by $c(\mathbf{y}, \mathbf{z}) := d(\mathbf{y}, \mathbf{z})^2/2$ the squared Riemannian distance between two points \mathbf{y} and \mathbf{z} on the unit hypersphere S^{d-1} ; both c and d are continuous and bounded. When equipped with the geodesic distance, S^{d-1} is a separable complete metric space, hence a Polish metric space, with Borel σ -field \mathcal{B}^{d-1} . Denote by λ^{d-1} the *surface area measure* over S^{d-1} . Throughout, measurability tacitly is understood with respect to \mathcal{B}^{d-1} and \mathbb{P} is assumed to be in the family \mathfrak{A}_d of λ^{d-1} -absolutely continuous distributions with densities bounded away from 0 and ∞ .

Measure transportation on Polish spaces and, more particularly, on Riemannian manifolds, is a well-studied subject; below, we mainly follow McCann (2001), Ambrosio and Pratelli (2003), and Schachermayer and Teichmann (2008). Let \mathbb{P} and \mathbb{Q} denote two probability measures on S^{d-1} . The Monge problem on S^{d-1} consists in minimizing, among the set $\mathcal{S}(\mathbb{P}, \mathbb{Q})$ of all measurable transport maps $\mathbf{S} : S^{d-1} \rightarrow S^{d-1}$ such that $(\mathbf{S}\#\mathbb{P})(V) := \mathbb{P}(\mathbf{S}^{-1}(V)) = \mathbb{Q}(V)$ for

all $V \in \mathcal{B}^{d-1}$ (in the measure transportation terminology, $\mathbf{S} \in \mathcal{S}(P, Q)$ is *pushing* P forward to Q), the transportation cost

$$C_M(\mathbf{S}) := \int_{S^{d-1}} c(\mathbf{z}, \mathbf{S}(\mathbf{z})) dP(\mathbf{z}) = E_P[c(\mathbf{Z}, \mathbf{S}(\mathbf{Z}))]. \quad (2.3)$$

Due to the fact that $\mathcal{S}(P, Q)$ is not convex, Monge's problem is an uneasy one.

Closely related to Monge's problem is the so-called Kantorovich problem. Denote by $\Gamma(P, Q)$ the set of all probability measures γ on $S^{d-1} \times S^{d-1}$ with "marginals" P and Q ; an element γ of $\Gamma(P, Q)$ is called a *transport plan*. The Kantorovich problem on S^{d-1} consists in minimizing, among all transport plans $\gamma \in \Gamma(P, Q)$, the expectation

$$C_K(\gamma) := \int_{S^{d-1} \times S^{d-1}} c(\mathbf{y}, \mathbf{z}) d\gamma(\mathbf{y}, \mathbf{z}) \quad (2.4)$$

of the transportation cost $c(\mathbf{Y}, \mathbf{Z})$ under $(\mathbf{Y}, \mathbf{Z}) \sim \gamma$. Unlike $\mathcal{S}(P, Q)$, the set $\Gamma(P, Q)$ is a convex subset of a Banach space; since c is bounded, the existence of a solution is guaranteed.

The Kantorovich problem is a relaxation of Monge's. Letting $(\mathbf{I}_d \times \mathbf{S})\mathbf{Z} := (\mathbf{Z}, \mathbf{S}(\mathbf{Z}))$, a transport map $\mathbf{S} \in \mathcal{S}(P, Q)$ indeed induces a transport plan $\gamma = (\mathbf{I}_d \times \mathbf{S})\#P \in \Gamma(P, Q)$ which is concentrated on the graph of \mathbf{S} (i.e., such that $\gamma((\mathbf{Z}, \mathbf{S}(\mathbf{Z})) \in \{(\mathbf{z}, \mathbf{S}(\mathbf{z})) : \mathbf{z} \in S^{d-1}\}) = 1$) and satisfying $C_K(\gamma) = C_M(\mathbf{S})$. As we shall see (Proposition 1 below), the solution of Kantorovich's problem is precisely of the form $(\mathbf{I}_d \times \mathbf{F})\#P$ where \mathbf{F} , thus, is a solution of Monge's problem, and

$$C_M(\mathbf{F}) = \min_{\mathbf{S} \in \mathcal{S}(P, Q)} C_M(\mathbf{S}) = \min_{\gamma \in \Gamma(P, Q)} C_K(\gamma) = C_K((\mathbf{I}_d \times \mathbf{F})\#P),$$

where $\min_{\gamma \in \Gamma(P, Q)} C_K^{1/2}(\gamma) := \mathcal{W}_2(P, Q)$ is the Wasserstein distance between P and Q .

Before providing more precise statements about the solutions of the Monge and Kantorovich problems, let us introduce some notation from differential geometry. Recall that the *tangent space* (tangent to S^{d-1}) at $\mathbf{x} \in S^{d-1}$ is the $(d-1)$ -dimensional linear subspace $\mathcal{T}_{\mathbf{x}}S^{d-1} := \{\mathbf{z} \in \mathbb{R}^d, \mathbf{z}^\top \mathbf{x} = 0\}$. Letting $\mathbf{x} \in S^{d-1}$ and $\mathbf{v} \in \mathcal{T}_{\mathbf{x}}S^{d-1}$, the directional derivative at $\mathbf{x} \in S^{d-1}$ of a smooth function $\zeta : S^{d-1} \rightarrow \mathbb{R}$ in direction \mathbf{v} is defined as $\nu(\zeta) := (\zeta \circ \nu)'(0)$, where $\nu : [0, 1] \rightarrow S^{d-1}$ is a differentiable path such that $\nu(0) = \mathbf{x}$ and $\nu'(0) = \mathbf{v}$. The gradient $\nabla_{\zeta}(\mathbf{x})$ of ζ at $\mathbf{x} \in S^{d-1}$ then is defined as the vector in $\mathcal{T}_{\mathbf{x}}S^{d-1}$ such that $\mathbf{v}^\top \nabla_{\zeta}(\mathbf{x}) = \nu(\zeta)$ for all $\mathbf{v} \in \mathcal{T}_{\mathbf{x}}S^{d-1}$ and $\mathbf{x} \in S^{d-1}$. The exponential map at a point $\mathbf{x} \in S^{d-1}$ is a map from the tangent space $\mathcal{T}_{\mathbf{x}}S^{d-1}$ to S^{d-1} . More precisely, denoting by $\nu_{\mathbf{v}}(t)$ the unique geodesic with tangent vector $\mathbf{v} \in \mathcal{T}_{\mathbf{x}}S^{d-1}$ running through $\mathbf{x} \in S^{d-1}$ ($\nu_{\mathbf{v}}(0) = \mathbf{x}$), then $\exp_{\mathbf{x}}(\mathbf{v}) := \nu_{\mathbf{v}}(1)$. Finally, consider the following concepts of *c-cyclical monotonicity* and *c-convexity*.

Definition 1 A subset $\Omega \in S^{d-1} \times S^{d-1}$ is called *c-cyclically monotone* (c the squared Riemannian distance on S^{d-1}) if, denoting by $\Sigma(k)$ the set of permutations of $\{1, \dots, k\}$, for all $k \in \mathbb{N}$, all $\sigma \in \Sigma(k)$, and all $(\mathbf{x}_1, \mathbf{y}_1), \dots, (\mathbf{x}_k, \mathbf{y}_k) \in \Omega$,

$$\sum_{i=1}^k c(\mathbf{x}_i, \mathbf{y}_i) \leq \sum_{i=1}^k c(\mathbf{x}_{\sigma(i)}, \mathbf{y}_i).$$

Definition 2 Two functions ψ and ϕ from S^{d-1} to \mathbb{R} such that

$$\psi(\mathbf{x}) = \sup_{\mathbf{y} \in S^{d-1}} \{\phi(\mathbf{y}) - c(\mathbf{x}, \mathbf{y})\} \text{ and } \phi(\mathbf{y}) = \inf_{\mathbf{x} \in S^{d-1}} \{\psi(\mathbf{x}) + c(\mathbf{x}, \mathbf{y})\} \quad (2.5)$$

are called *c-convex* and *c-concave*, respectively; call ϕ (resp. ψ) the *c-transform* of ψ (resp. ϕ).

Since the squared Riemannian distance c satisfies the conditions of Theorem 10.26(i) of Villani (2009), the functions ψ

and ϕ in (2.5) are a.e. differentiable. The following theorem summarizes, for the Monge and Kantorovich problems with transportation cost the squared Riemannian distance on S^{d-1} , some of the results contained in Chapter 5 of Villani (2009) (for the necessity part of (i), first established by Rüschemdorf (1996)), Theorem 1 of Schachermayer and Teichmann (2008) (for the sufficiency part of (i); see also Pratelli (2008)), Theorems 8 and 9 and Corollary 10 of McCann (2001) (for (ii), (iii), and (iv)). The assumptions made in these references are automatically satisfied here, since S^{d-1} equipped with the geodesic distance is a Polish metric space and c is a continuous bounded cost function.

Proposition 1 *Let $P \in \mathfrak{P}_d$ and Q denote two probability measures on S^{d-1} . Then,*

- (i) *a transport plan $\gamma \in \Gamma(P, Q)$ is the solution (minimizing C_K in (2.4) over $\Gamma(P, Q)$) of the Kantorovich problem if and only if it is supported on a c -cyclically monotone subset of $S^{d-1} \times S^{d-1}$;*
- (ii) *this solution of the Kantorovich problem exists, is unique, and is of the form $(I_d \times F)\#P$ where $F \in \mathcal{S}(P, Q)$ is the P -a.s. unique solution of the corresponding Monge problem (minimizing C_M in (2.3) over $\mathcal{S}(P, Q)$);*
- (iii) *there exist c -concave differentiable mappings ψ from S^{d-1} to \mathbb{R} such that $F(x) = \exp_x(-\nabla\psi(x))$, λ^{d-1} -a.e.*

If, moreover, $Q \in \mathfrak{P}_d$, then

- (iv) *$Q(x) := \exp_x(-\nabla\phi(x))$, with ϕ the c -transform of ψ , belongs to $\mathcal{S}(Q, P)$, is the Q -a.s. unique minimizer of C_M in (2.3) over $\mathcal{S}(Q, P)$ (i.e., the Q -a.s. unique solution of the corresponding Monge problem), and satisfies*

$$Q(F(x)) = x \quad P\text{-a.s.} \quad \text{and} \quad F(Q(x)) = x \quad Q\text{-a.s.}$$

Proposition 1 entails the existence of a mapping F pushing any probability measure $P \in \mathfrak{P}_d$ forward to any other probability measure $Q \in \mathfrak{P}_d$ and minimizing, among all such mappings, the transportation cost (2.3). In the next Section, we will use this optimality result to define directional distribution and quantile functions.

3 — DIRECTIONAL DISTRIBUTION AND QUANTILE FUNCTIONS

3.1 — Definitions and some basic properties

The concepts of directional distribution and quantile functions we are proposing are based on the optimal transport F from a generic probability measure $P \in \mathfrak{P}_d$ to the uniform probability measure P^U on S^{d-1} . The idea is inspired by the so-called *center-outward distribution* and *quantile functions* F_\pm and $Q_\pm := F_\pm^{-1}$ introduced in Hallin et al. (2021a) for distributions on \mathbb{R}^d , which involve optimal transports to the spherical uniform over the unit ball. On the hypersphere, the definition of the *directional distribution function* of a random vector $Z \sim P^Z \in \mathfrak{P}_d$ with values on S^{d-1} is as follows (we indifferently use the expressions *directional distribution and quantile functions of Z* and *directional distribution and quantile functions of P^Z*).

Definition 3 *Call (directional) distribution function of $P^Z \in \mathfrak{P}_d$ the a.s. unique optimal transport map F from S^{d-1} to S^{d-1} such that $F\#P^Z = P^U$.*

This definition is very natural, since F of $Z \sim P^Z$ is such that $F(Z) \sim P^U$ —so that F has the same probability integral transformation flavor as classical univariate distribution functions. We then have the following important property (see the Appendix for a proof).

Proposition 2 *The distribution function F of $Z \sim P^Z \in \mathfrak{P}_d$ is a homeomorphism from S^{d-1} to S^{d-1} .*

It directly follows from Proposition 2 that the inverse $Q := F^{-1}$ of F is well defined, which yields the following definition of a *directional quantile function*.

Definition 4 Call $\mathbf{Q} := \mathbf{F}^{-1}$ the directional quantile function of $\mathbf{P}^{\mathbf{Z}} \in \mathfrak{P}_d$.

In \mathbb{R}^d , the center-outward distribution function \mathbf{F}_{\pm} was defined as an optimal transport to the spherical uniform \mathbf{U}_d over the unit ball of \mathbb{R}^d . For \mathbf{U}_d , nested balls of the form $\tau \mathcal{S}^{d-1}$, centered at the origin and with \mathbf{U}_d -probability contents τ , naturally play the role of quantile regions of order $\tau \in [0, 1]$; the origin thus naturally qualifies as the median of \mathbf{U}_d . The center-outward quantile regions then are obtained as the images by $\mathbf{Q}_{\pm} := \mathbf{F}_{\pm}^{-1}$ of these balls.

The basic idea is quite similar in \mathcal{S}^{d-1} . If, however, nested regions with $\mathbf{P}^{\mathbf{U}}$ -probability contents $\tau \in [0, 1]$ are to be defined on \mathcal{S}^{d-1} , a central point or pole $\boldsymbol{\theta} \in \mathcal{S}^{d-1}$ has to be chosen, playing the role of a directional median for $\mathbf{P}^{\mathbf{Z}}$. Since the uniform $\mathbf{P}^{\mathbf{U}}$ automatically enjoys rotational symmetry with respect to the image $\mathbf{F}(\boldsymbol{\theta})$ of that pole, the nested regions playing the role of $\mathbf{P}^{\mathbf{U}}$ -quantile regions should be invariant with respect to rotations with axis $\mathbf{F}(\boldsymbol{\theta})$: hence, the collection of spherical caps with $\mathbf{P}^{\mathbf{U}}$ -probability contents τ centered at $\mathbf{F}(\boldsymbol{\theta})$ naturally qualifies as the family of (nested) quantile regions of orders $\tau \in [0, 1]$ of $\mathbf{P}^{\mathbf{U}}$.

The choice of a directional median or pole $\boldsymbol{\theta}$, of course, should be $\mathbf{P}^{\mathbf{Z}}$ -specific. The literature on directional data provides several concepts of *directional medians*, the most convenient of which is the so-called *Fréchet mean* of $\mathbf{Z} \sim \mathbf{P}^{\mathbf{Z}}$, defined as

$$\boldsymbol{\theta}_{\text{Fr}} := \operatorname{argmin}_{\mathbf{z} \in \mathcal{S}^{d-1}} \mathbb{E}_{\mathbf{P}^{\mathbf{Z}}} [c(\mathbf{Z}, \mathbf{z})] \quad (3.6)$$

(recall that $c(\mathbf{z}_1, \mathbf{z}_2)$ denotes the squared Riemannian distance between \mathbf{z}_1 and \mathbf{z}_2). The Fréchet mean always exists but is not necessarily unique. In case (3.6) has multiple solutions, one can randomly select $\boldsymbol{\theta}$ as one of them.

Another possible choice can be based on the transport map \mathbf{F} (equivalently, on the quantile function \mathbf{Q}) itself. For each $\mathbf{z} \in \mathcal{S}^{d-1}$, consider the hyper-hemi-sphere $\mathcal{H}_{\mathbf{z}} := \{\mathbf{u} \in \mathcal{S}^{d-1} : \mathbf{u}^{\top} \mathbf{F}(\mathbf{z}) \geq 0\}$ centered at $\mathbf{F}(\mathbf{z})$. Since \mathbf{F} pushes $\mathbf{P}^{\mathbf{Z}}$ forward to $\mathbf{P}^{\mathbf{U}}$, we have that $\mathbf{P}^{\mathbf{U}}(\mathcal{H}_{\mathbf{z}}) = \mathbf{P}^{\mathbf{Z}}(\mathbf{Q}(\mathcal{H}_{\mathbf{z}})) = 1/2$. In general, however, $\mathbf{Q}(\mathcal{H}_{\mathbf{z}})$ is not a hyper-hemisphere and $1/2 = \mathbf{P}^{\mathbf{U}}(\mathcal{H}_{\mathbf{z}}) \neq \mathbf{P}^{\mathbf{U}}(\mathbf{Q}(\mathcal{H}_{\mathbf{z}}))$. A transport-based concept of median for $\mathbf{P}^{\mathbf{Z}}$ is thus

$$\boldsymbol{\theta}_{\text{Tr}} := \operatorname{argmin}_{\mathbf{z} \in \mathcal{S}^{d-1}} \mathbf{P}^{\mathbf{U}}(\mathbf{Q}(\mathcal{H}_{\mathbf{z}})). \quad (3.7)$$

This directional median or pole $\boldsymbol{\theta}_{\text{Tr}}$ indeed is such that the area of the image by \mathbf{Q} of the hyper-hemisphere centered at $\mathbf{F}(\boldsymbol{\theta}_{\text{Tr}})$ is minimal among the areas of all images $\mathbf{Q}(\mathcal{H}_{\mathbf{z}})$ of hyper-hemispheres, indicating a concentration of the $\mathbf{P}^{\mathbf{Z}}$ probability mass around $\boldsymbol{\theta}_{\text{Tr}}$. This pole always exists. Again, it may not be unique and one can randomly select $\boldsymbol{\theta}$ within the set of points satisfying (3.7).

Assume that a pole $\boldsymbol{\theta}_{\text{M}}$, say, has been selected for $\mathbf{P}^{\mathbf{Z}}$ ($\boldsymbol{\theta}_{\text{Fr}}$ or $\boldsymbol{\theta}_{\text{Tr}}$ being possible choices). The spherical cap with $\mathbf{P}^{\mathbf{U}}$ -probability τ centered at $\mathbf{F}(\boldsymbol{\theta}_{\text{M}})$ is

$$\mathbb{C}_{\tau}^{\mathbf{U}} := \left\{ \mathbf{u} \in \mathcal{S}^{d-1} : F_{*}(\mathbf{u}^{\top} \mathbf{F}(\boldsymbol{\theta}_{\text{M}})) \geq 1 - \tau \right\} \quad 0 \leq \tau \leq 1,$$

with boundary

$$\mathbb{C}_{\tau}^{\mathbf{U}} := \left\{ \mathbf{u} \in \mathcal{S}^{d-1} : F_{*}(\mathbf{u}^{\top} \mathbf{F}(\boldsymbol{\theta}_{\text{M}})) = 1 - \tau \right\} \quad 0 \leq \tau \leq 1, \quad (3.8)$$

(a $(d-2)$ -dimensional hypersphere) where

$$F_{*}(u) := \int_{-1}^u (1-s^2)^{(d-3)/2} ds \Big/ \int_{-1}^1 (1-s^2)^{(d-3)/2} ds, \quad -1 \leq u \leq 1. \quad (3.9)$$

Indeed, it is easy to see that $u \mapsto F_*(u)$ is the distribution function of $\mathbf{U}^\top \mathbf{F}(\boldsymbol{\theta}_M)$ where $\mathbf{U} \sim \mathbf{P}^{\mathbf{U}}$. Hence, $F_*(\mathbf{u}^\top \mathbf{F}(\boldsymbol{\theta}_M))$ is the $\mathbf{P}^{\mathbf{U}}$ -probability of the $\mathbf{F}(\boldsymbol{\theta}_M)$ -centered spherical cap running through \mathbf{u} and a measure of \mathbf{u} 's latitude, ranging from 0 (for $\mathbf{u} = -\mathbf{F}(\boldsymbol{\theta}_M)$) to 1 (for $\mathbf{u} = \mathbf{F}(\boldsymbol{\theta}_M)$) and scaled in such a way that the latitude of $\mathbf{U} \sim \mathbf{P}^{\mathbf{U}}$ is uniform over $[0, 1]$. Therefore, for the hypersphere S^{d-1} equipped with the uniform distribution $\mathbf{P}^{\mathbf{U}}$ and the pole $\mathbf{F}(\boldsymbol{\theta}_M)$, the contour $C_\tau^{\mathbf{U}}$ plays the role of a *parallel* of order τ ($C_{1/2}^{\mathbf{U}}$, thus, is an *equatorial hypersphere*).

Accordingly, define the quantile contour and quantile region of order τ of $\mathbf{Z} \sim \mathbf{P}^{\mathbf{Z}}$ as the images

$$C_\tau := \mathbf{Q} \left(C_\tau^{\mathbf{U}} \right) = \left\{ \mathbf{z} \in S^{d-1} : F_* \left(\mathbf{F}^\top(\mathbf{z}) \mathbf{F}(\boldsymbol{\theta}_M) \right) = 1 - \tau \right\} \quad (3.10)$$

and

$$C_\tau := \mathbf{Q} \left(C_\tau^{\mathbf{U}} \right) = \left\{ \mathbf{z} \in S^{d-1} : F_* \left(\mathbf{F}^\top(\mathbf{z}) \mathbf{F}(\boldsymbol{\theta}_M) \right) \geq 1 - \tau \right\}, \quad (3.11)$$

by \mathbf{Q} of $C_\tau^{\mathbf{U}}$ and $C_\tau^{\mathbf{U}}$, respectively. Since \mathbf{Q} is a measure-preserving transformation pushing $\mathbf{P}^{\mathbf{U}}$ forward to $\mathbf{P}^{\mathbf{Z}}$, the $\mathbf{P}^{\mathbf{Z}}$ probability content of C_τ is τ . The following proposition summarizes the main properties of \mathbf{F} , \mathbf{Q} , the quantile contours C_τ and quantile regions C_τ . They all follow from the definitions and the continuity of \mathbf{F} and \mathbf{Q} .

Proposition 3 Let $\mathbf{Z} \sim \mathbf{P}^{\mathbf{Z}} \in \mathfrak{P}_d$ have distribution and quantile functions \mathbf{F} and \mathbf{Q} , respectively. Then,

- (i) \mathbf{F} entirely characterizes $\mathbf{P}^{\mathbf{Z}}$, $\mathbf{F}(\mathbf{Z}) \sim \mathbf{F} \# \mathbf{P}^{\mathbf{Z}} = \mathbf{P}^{\mathbf{U}}$, and $F_* \left((\mathbf{F}^\top(\mathbf{Z})) \mathbf{F}(\boldsymbol{\theta}_M) \right) \sim \mathbf{U}_{[0,1]}$;
- (ii) \mathbf{Q} entirely characterizes $\mathbf{P}^{\mathbf{Z}}$ and $\mathbf{Q}(\mathbf{U}) \sim \mathbf{Q} \# \mathbf{P}^{\mathbf{U}} = \mathbf{P}^{\mathbf{Z}}$;
- (iii) the quantile contours C_τ , $\tau \in [0, 1]$ are continuous; the quantile regions C_τ are closed, connected, and nested; their intersection $\bigcap_{\tau \in [0,1]} C_\tau$ is the directional median $\boldsymbol{\theta}_M$;
- (iv) the probability content $\mathbf{P}^{\mathbf{Z}}(C_\tau)$ of C_τ is τ , irrespective of $\mathbf{P}^{\mathbf{Z}} \in \mathfrak{P}_d$, $\tau \in [0, 1]$.

3.2 — A natural distribution-specific coordinate system

The quantile function \mathbf{Q} of $\mathbf{P}^{\mathbf{Z}}$ actually creates over S^{d-1} a coordinate system with latitudes and (hyper)longitudes adapted to the distribution of \mathbf{Z} .

The usual latitude-(hyper)longitude coordinate system is based on the classical *tangent-normal* decomposition, with respect to a pole $\mathbf{F}(\boldsymbol{\theta}_M)$, say, of a point $\mathbf{u} \in S^{d-1}$ into the sum of two mutually orthogonal terms

$$\mathbf{u} = (\mathbf{u}^\top \mathbf{F}(\boldsymbol{\theta}_M)) \mathbf{F}(\boldsymbol{\theta}_M) + (\mathbf{I}_d - \mathbf{F}(\boldsymbol{\theta}_M) \mathbf{F}^\top(\boldsymbol{\theta}_M)) \mathbf{u} = (\mathbf{u}^\top \mathbf{F}(\boldsymbol{\theta}_M)) \mathbf{F}(\boldsymbol{\theta}_M) + \sqrt{1 - (\mathbf{u}^\top \mathbf{F}(\boldsymbol{\theta}_M))^2} \mathbf{S}_{\mathbf{F}(\boldsymbol{\theta}_M)}(\mathbf{u}) \quad (3.12)$$

(see the left panel of Figure 1 for $d = 3$) where $\mathbf{u}^\top \mathbf{F}(\boldsymbol{\theta}_M)$, being constant over the parallel $C_\tau^{\mathbf{U}}$ ($\tau = 1 - F_*(\mathbf{u}^\top \mathbf{F}(\boldsymbol{\theta}_M))$) defined in Section 3.1, is a latitude while the unit vector (a *directional sign*)

$$\mathbf{S}_{\mathbf{F}(\boldsymbol{\theta}_M)}(\mathbf{u}) := (\mathbf{u} - (\mathbf{u}^\top \mathbf{F}(\boldsymbol{\theta}_M)) \mathbf{F}(\boldsymbol{\theta}_M)) / \|\mathbf{u} - (\mathbf{u}^\top \mathbf{F}(\boldsymbol{\theta}_M)) \mathbf{F}(\boldsymbol{\theta}_M)\| \quad (3.13)$$

(with the convention $\mathbf{0}/0 = \mathbf{0}$ for $\mathbf{u} = \pm \mathbf{F}(\boldsymbol{\theta}_M)$) with values on the equatorial hypersphere $C_{1/2}^{\mathbf{U}}$ —a hyperlongitude, thus—characterizes hypermeridians $\mathcal{M}_s^{\mathbf{U}} := \left\{ \mathbf{u} \in S^{d-1} : \mathbf{S}_{\mathbf{F}(\boldsymbol{\theta}_M)}(\mathbf{u}) = \mathbf{s} \right\}$, $\mathbf{s} \in C_{1/2}^{\mathbf{U}}$.

This parallel/hypermeridian system is well adapted to S^{d-1} when equipped with the surface area measure or the uniform measure $\mathbf{P}^{\mathbf{U}}$: parallels, for instance, then coincide with $\mathbf{P}^{\mathbf{U}}$'s quantile contours $C_\tau^{\mathbf{U}}$, while the hyperlongitudes $\mathbf{S}_{\mathbf{F}(\boldsymbol{\theta}_M)}(\mathbf{U})$, for $\mathbf{U} \sim \mathbf{P}^{\mathbf{U}}$, are uniform over the equatorial hypersphere. Its image by \mathbf{Q} is more natural under the probability measure $\mathbf{P}^{\mathbf{Z}}$: the same properties, indeed, then hold for the “curvilinear” parallels $\mathbf{Q}(C_\tau^{\mathbf{U}}) = C_\tau$ and the “curvilinear” hypermeridians

$$M_s := Q(M_s^U) := \{z \in S^{d-1} : \mathbf{S}_{F(\theta_M)}(F(z)) = s\}, \quad s \in C_{1/2}^U. \quad (3.14)$$

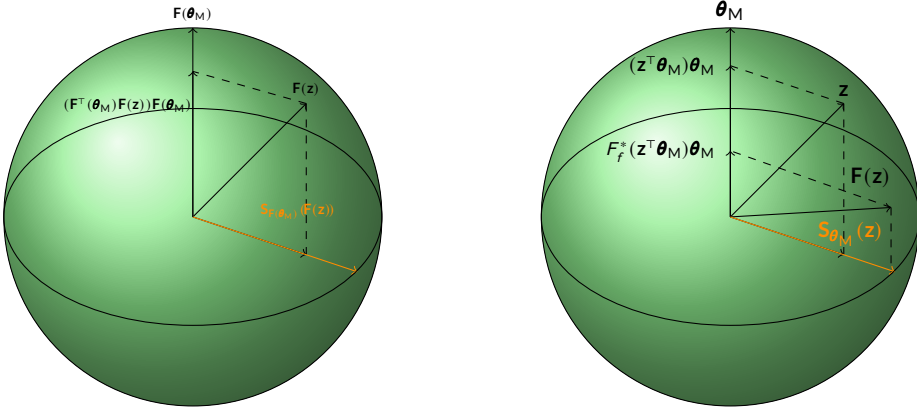


FIGURE 1 Left: The tangent-normal decomposition of F with respect to $F(\theta_M)$. Right: In the rotationally symmetric case, the optimal transport F reduces to an optimal univariate transport acting on the projection $z^T \theta_M$ of z along the rotation axis θ_M .

3.3 — Rotational symmetry

Optimal transports seldom admit closed-form expressions. In the particular case of rotational symmetry, however, explicit expressions for F and Q are possible.

Consider the rotationally symmetric variable $Z \sim P^Z$ with uniquely defined axis $\pm \theta$; all sensible directional medians θ_M (including θ_{Fr} and θ_{Tr}) then are such that θ_M is lying along that axis, and P^Z has density (1.2) with $\theta = \theta_M$: write $P^Z = P_{\theta_M, f}$. Denote by

$$F_f(u) := \int_{-1}^u f(s)(1-s^2)^{(\rho-3)/2} ds / \int_{-1}^1 f(s)(1-s^2)^{(\rho-3)/2} ds, \quad -1 \leq u \leq 1,$$

the distribution function of $Z^T \theta_M$, by $Q_f := F_f^{-1}$ its quantile function. Under rotational symmetry, we have that

$$\mathbf{S}_{\theta_M}(Z) = (Z - (Z^T \theta_M) \theta_M) / \|Z - (Z^T \theta_M) \theta_M\| \quad (3.15)$$

(with the convention that $0/0 = 0$) is uniformly distributed over the *equatorial hypersphere* (see, e.g., [Paindaveine and Verdebout \(2017\)](#))

$$S_{\theta_M}^{d-2} := \{u \in \mathbb{R}^d : u^T \theta_M = 0, u^T u = 1\}. \quad (3.16)$$

Actually, $\mathbf{S}_{\theta_M}(z)$ is the point in the equatorial sphere with the same *hyperlongitudes* as z and can be interpreted as the *directional sign* of z . Since $F(Z)$ by definition is uniform over S^{d-1} , $F^T(Z) \theta_M$ has distribution function F_* as defined in (3.9) and quantile function $Q_* = F_*^{-1}$. We then have an explicit form for the directional distribution function F of $Z \sim P_{\theta_M, f}$ (see Appendix 7.2 for a proof).

Proposition 4 Let \mathbf{Z} have rotationally symmetric distribution $\mathbb{P}_{\boldsymbol{\theta}_M, f}$. Then, letting $F_f^*(u) := Q_*(F_f(u))$,

$$\mathbf{F}(\mathbf{z}) = F_f^*(\mathbf{z}^\top \boldsymbol{\theta}_M) \boldsymbol{\theta}_M + \sqrt{1 - (F_f^*(\mathbf{z}^\top \boldsymbol{\theta}_M))^2} \mathbf{S}_{\boldsymbol{\theta}_M}(\mathbf{z}). \quad (3.17)$$

Proposition 4 tells us that, in the rotationally symmetric case, the optimal transport \mathbf{F} essentially reduces to the optimal univariate transport, the function F_f^* acting on the projection $\mathbf{z}^\top \boldsymbol{\theta}_M$ of \mathbf{z} onto the axis $\boldsymbol{\theta}_M$. This is illustrated in Figure 1 (right panel). Again, this explains—but does not justify—the ubiquity, in directional statistics, of the rotational symmetry assumption: just as the assumption of ellipticity in \mathbb{R}^d , rotational symmetry, when it holds true, actually reduces complex multivariate problems to much simpler univariate ones.

4 — EMPIRICAL DISTRIBUTION AND QUANTILE FUNCTIONS, RANKS, AND SIGNS

So far, we have been dealing with population concepts only. If a statistical analysis is to be performed, we need empirical versions of the same.

4.1 — Empirical directional distribution function

Denoting by $\mathbf{Z}_1^{(n)}, \dots, \mathbf{Z}_n^{(n)}$ a sample of n i.i.d. observations with distribution $\mathbb{P}^{\mathbf{Z}}$, consider a “regular” n -point grid $\mathbb{G}^{(n)} = \{\omega_1^{(n)}, \dots, \omega_n^{(n)}\}$ over the unit hypersphere S^{d-1} . In this section, the only property required from $\mathbb{G}^{(n)}$ is that the uniform over its n gridpoints converges weakly to the uniform distribution $\mathbb{P}^{\mathbf{U}}$ over S^{d-1} as $n \rightarrow \infty$.

Since \mathbf{F} minimizes the transportation cost (2.3), a plugin estimator is obtained as the solution of an optimal coupling problem between the observations and the grid $\mathbb{G}^{(n)}$. More precisely, let $\mathcal{T}^{(n)}$ denote the set of all permutations of the integers $\{1, \dots, n\}$: each permutation $T \in \mathcal{T}^{(n)}$ defines a bijection $\mathbf{Z}_i^{(n)} \mapsto \omega_{T(i)}^{(n)}$ between $\{\mathbf{Z}_1^{(n)}, \dots, \mathbf{Z}_n^{(n)}\}$ and $\mathbb{G}^{(n)}$. The *empirical directional distribution function* $\mathbf{F}^{(n)}$ is then defined as the mapping

$$\mathbf{F}^{(n)} : \mathbf{Z}^{(n)} := (\mathbf{Z}_1^{(n)}, \dots, \mathbf{Z}_n^{(n)}) \mapsto (\mathbf{F}^{(n)}(\mathbf{Z}_1^{(n)}), \dots, \mathbf{F}^{(n)}(\mathbf{Z}_n^{(n)})) \quad (4.18)$$

satisfying (with $c(\mathbf{z}_1, \mathbf{z}_2)$ the squared Riemannian distance)

$$\sum_{i=1}^n c(\mathbf{Z}_i^{(n)}, \mathbf{F}^{(n)}(\mathbf{Z}_i^{(n)})) = \min_{T \in \mathcal{T}^{(n)}} \sum_{i=1}^n c(\mathbf{Z}_i^{(n)}, \omega_{T(i)}^{(n)}). \quad (4.19)$$

The terminology *empirical directional distribution function* is justified by the following Glivenko-Cantelli result (see Appendix 7.2 for a proof).

Proposition 5 (Glivenko-Cantelli). Let $\mathbf{Z}_1^{(n)}, \dots, \mathbf{Z}_n^{(n)}$ be i.i.d. with distribution $\mathbb{P}^{\mathbf{Z}}$ over S^{d-1} . Then, provided that the uniform discrete distribution over the n grid-points $\{\omega_1^{(n)}, \dots, \omega_n^{(n)}\}$ of $\mathbb{G}^{(n)}$ converges weakly, as $n \rightarrow \infty$, to the uniform distribution $\mathbb{P}^{\mathbf{U}}$ over S^{d-1} ,

$$\max_{1 \leq i \leq n} \|\mathbf{F}^{(n)}(\mathbf{Z}_i^{(n)}) - \mathbf{F}(\mathbf{Z}_i^{(n)})\| \longrightarrow 0 \quad \text{almost surely as } n \rightarrow \infty. \quad (4.20)$$

If a consistent estimation of \mathbf{F} is the objective, the empirical distribution $\mathbf{F}^{(n)}$ defined in (4.18), in view of (4.20),

offers a perfect solution. If empirical counterparts of the quantile contours and regions C_τ and \mathbb{C}_τ , hence of the parallels C_τ and hypermeridians \mathcal{M}_s (see (3.8) and (3.14)) of Section 3.2 are to be constructed, or if ranks and signs generating a maximal ancillary sigma-field are to be defined, however, more structure is required from the grid $\mathbb{G}^{(n)}$.

4.2 — Directional ranks, signs, and empirical quantiles

In this subsection, we show how imposing some additional finite- n structure on the grid $\mathbb{G}^{(n)}$ yields empirical versions of \mathbf{F} with natural data-driven concepts of

- (i) empirical quantile contours and regions consistently estimating the actual ones,
- (ii) a data-driven coordinate system of empirical parallels and hypermeridians adapting to the underlying distribution \mathbb{P}^Z of the observations, and
- (iii) distribution-free signs and ranks, paving the way to a theory of rank-based inference for directional data with unspecified density.

All these concepts involve a pole θ_M (the population Fréchet mean, for instance) or a consistent estimator $\widehat{\theta}_M^{(n)}$ thereof (e.g., the empirical Fréchet mean). That $\widehat{\theta}_M^{(n)}$ in turn will define the pole $\widehat{\theta}^{(n)}$ of a structured grid $\mathbb{G}^{(n)}(\widehat{\theta}^{(n)})$ to be used in the estimation of \mathbf{F} . Accordingly, we are proceeding in two steps: a first step yielding an empirical pole $\widehat{\theta}^{(n)}$, then a second step estimating \mathbf{F} on the basis of the grid $\mathbb{G}^{(n)}(\widehat{\theta}^{(n)})$ exploiting the role of $\widehat{\theta}^{(n)}$ as an empirical pole.

Step 1. Construct an empirical version $\widehat{\theta}^{(n)}$ of the population quantity $\mathbf{F}(\theta_M)$. Let $\widehat{\theta}_M^{(n)}$ be a consistent estimator of θ_M and consider an n -point grid $\mathbb{G}_0^{(n)}$ satisfying the assumptions of Proposition 5; denoting by $\mathbf{F}_0^{(n)}(\mathbf{Z}_i^{(n)})$ the resulting estimator of $\mathbf{F}(\mathbf{Z}_i^{(n)})$, choose $\widehat{\theta}^{(n)} := \mathbf{F}_0^{(n)}(\mathbf{Z}_i^{(n)})$ where $\mathbf{Z}_i^{(n)}$ is the sample point closest to $\widehat{\theta}_M^{(n)}$ in the $d(\cdot, \cdot)$ metric: Proposition 5 and the continuity of \mathbf{F} imply that $\widehat{\theta}^{(n)}$ a.s. converges to $\mathbf{F}(\theta_M)$.

Step 2. (2a) Construct a further regular grid $\mathbb{G}^{(n)}(\widehat{\theta}^{(n)})$ over \mathcal{S}^{d-1} . Factorizing n into $n = n_R n_S + n_0$ where $n_R, n_S, n_0 \in \mathbb{N}$ and $0 \leq n_0 < \min\{n_R, n_S\}$, define that grid $\mathbb{G}^{(n)}(\widehat{\theta}^{(n)})$ as the product of two independent grids:

- (i) a reference grid $\mathbb{E}^{(n_S)} := \{\mathbf{s}_1, \dots, \mathbf{s}_{n_S}\}$ over \mathcal{S}^{d-2} ; again, this grid should be as uniform as possible but the only requirement is the weak convergence, as $n_S \rightarrow \infty$, of the uniform distribution over $\mathbb{E}^{(n_S)}$ to the uniform over \mathcal{S}^{d-2} . Note that for $d = 3$, a fully regular grid $\mathbf{s}_1, \dots, \mathbf{s}_{n_S}$ is obtained by dividing the unit circle \mathcal{S}^1 into n_S equal parts (see Figure 2);
- (ii) a grid of n_R points over the unit interval, of the form $i/(n_R + 1)$, $i = 1, \dots, n_R$.

(2b) Import the grid $\mathbb{E}^{(n_S)}$ of step (2a) to the equatorial space defined by the pole $\widehat{\theta}^{(n)}$ computed in step 1. More precisely, construct the grid $\mathbb{G}^{(n)}(\widehat{\theta}^{(n)})$ that consists in n_0 copies of $\widehat{\theta}^{(n)}$ (if $n_0 \neq 0$) and the $n_R n_S$ points $\mathbb{G}_{ij}^{(n)}(\widehat{\theta}^{(n)})$ such that

$$1 - F_*((\mathbb{G}_{ij}^{(n)}(\widehat{\theta}^{(n)}))^{\top} \widehat{\theta}^{(n)}) = \frac{i}{n_R + 1} \quad \text{and} \quad \mathbf{S}_{\widehat{\theta}^{(n)}}(\mathbb{G}_{ij}^{(n)}(\widehat{\theta}^{(n)})) = \Gamma_{\widehat{\theta}^{(n)}} \mathbf{s}_j, \quad i = 1, \dots, n_R, j = 1, \dots, n_S$$

where $\Gamma_{\widehat{\theta}}$ denotes a $d \times (d - 1)$ semi-orthogonal matrix such that $\Gamma_{\widehat{\theta}} \Gamma_{\widehat{\theta}}^{\top} = \mathbf{I}_d - \widehat{\theta} \widehat{\theta}^{\top}$ and $\Gamma_{\widehat{\theta}}^{\top} \Gamma_{\widehat{\theta}} = \mathbf{I}_{d-1}$; the columns of $(\widehat{\theta}^{(n)}, \Gamma_{\widehat{\theta}^{(n)}}^{\top})$, thus, constitute an orthonormal coordinate system of \mathbb{R}^d , the columns of $\Gamma_{\widehat{\theta}^{(n)}}^{\top}$ an arbitrary orthonormal coordinate system of the equatorial hyperplane determined by $\widehat{\theta}^{(n)}$. Note that, due to its dependence on $\widehat{\theta}^{(n)}$, this grid $\mathbb{G}^{(n)}(\widehat{\theta}^{(n)})$ is random.

(2c) Denote by $\mathbf{F}^{(n)}(\mathbf{Z}_1^{(n)}), \dots, \mathbf{F}^{(n)}(\mathbf{Z}_n^{(n)})$ the solutions of the optimal coupling problem (4.19) based on this second grid $\mathbb{G}^{(n)}(\widehat{\theta}^{(n)})$ constructed in the previous step.

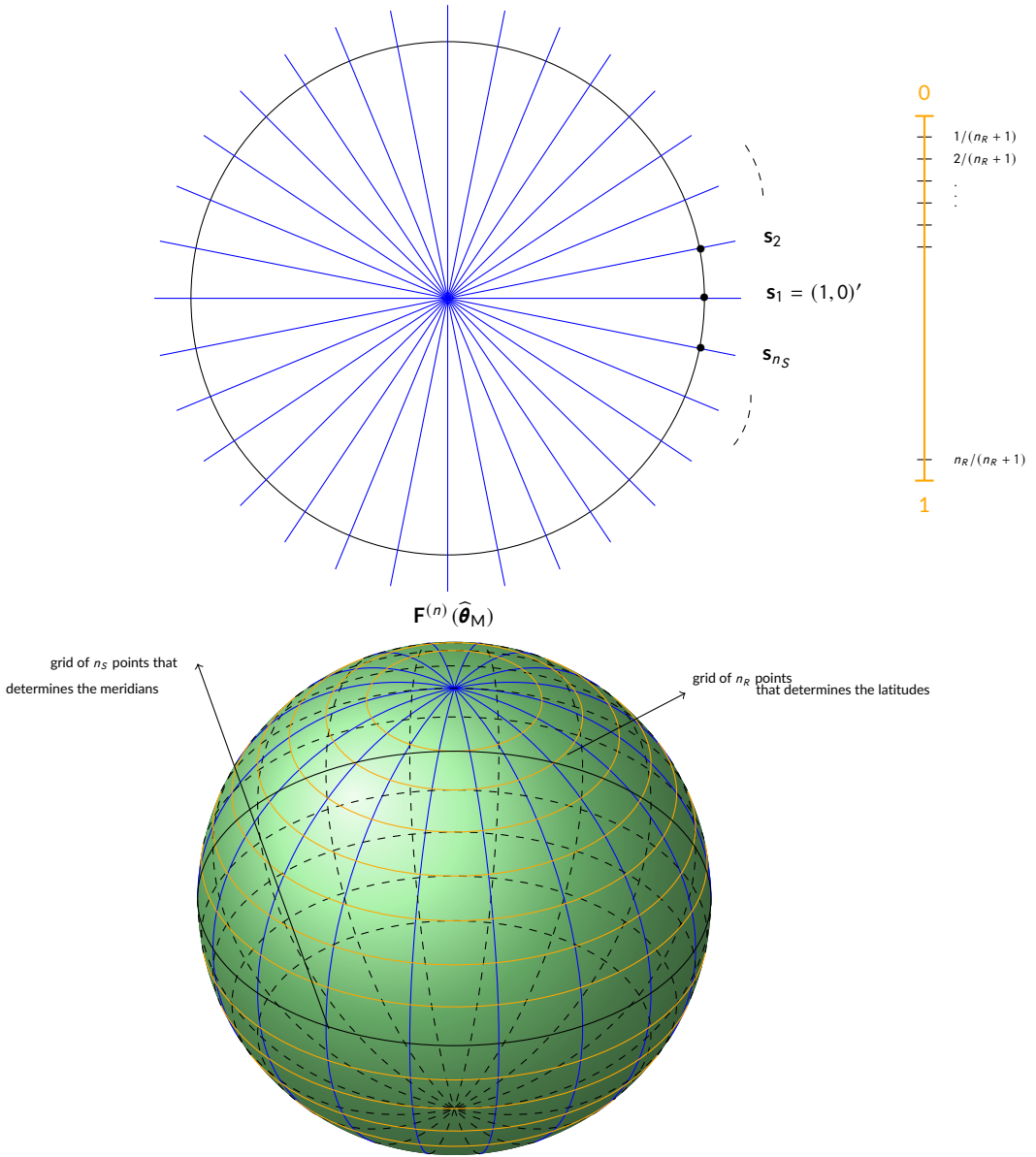


FIGURE 2 The grid used to define signs and ranks on S^{d-1} for $d = 3$. The final grid is obtained as the product of a reference grid $\mathfrak{S}^{(n_S)} := \{\mathbf{s}_1, \dots, \mathbf{s}_{n_S}\}$ over S^{d-2} (here, n_S equispaced points on the circle S^1) and n_R equispaced points on the unit interval.

The (directional) empirical sign $\mathbf{S}_i^{(n)}$ and the (directional) rank $R_i^{(n)}$ of $\mathbf{Z}_i^{(n)}$ then are naturally defined as

$$\mathbf{S}_i^{(n)} := \mathbf{S}_{\hat{\theta}_n}(\mathbf{F}^{(n)}(\mathbf{Z}_i^{(n)})) \quad (4.21)$$

and

$$R_i^{(n)} = R^{(n)}(\mathbf{Z}_i^{(n)}) := (n_R + 1) \left[1 - F_*((\mathbf{F}^{(n)}(\mathbf{Z}_i^{(n)}))^{\top} \hat{\boldsymbol{\theta}}^{(n)}) \right], \quad i = 1, \dots, n \quad (4.22)$$

(with values in $\{1, \dots, n_R\}$), respectively, provided that $\mathbf{F}^{(n)}(\mathbf{Z}_i^{(n)}) \neq \widehat{\boldsymbol{\theta}}^{(n)}$; for $\mathbf{Z}_i^{(n)}$ such that $\mathbf{F}^{(n)}(\mathbf{Z}_i^{(n)}) = \widehat{\boldsymbol{\theta}}^{(n)}$, let $\mathbf{S}_i^{(n)} := \mathbf{0}$ (the pole has no specific longitude) and $\mathcal{R}_i^{(n)} := 0$.

The empirical versions of the quantile contours and regions (3.10) and (3.11) are the collections of observations

$$\mathcal{C}_{j/(n_R+1)}^{(n)} := \left\{ \mathbf{Z}_i^{(n)} : \mathcal{R}_i^{(n)} = j \right\} \quad \text{and} \quad \mathcal{C}_{j/(n_R+1)}^{(n)} := \left\{ \mathbf{Z}_i^{(n)} : \mathcal{R}_i^{(n)} \leq j \right\}, \quad j = 1, \dots, n_R, \quad (4.23)$$

respectively. An empirical quantile contour of order $j/(n_R+1)$ (the empirical parallel of order $j/(n_R+1)$) thus consists of the n_S sample points with given rank j . Similarly, the empirical hypermeridian with longitude \mathbf{s} consists of the n_R observations with given sign (hyperlongitude) \mathbf{s} :

$$\mathcal{M}_{\mathbf{s}}^{(n)} := \left\{ \mathbf{Z}_i^{(n)} : \mathbf{F}^{(n)}(\mathbf{Z}_i^{(n)}) \neq \widehat{\boldsymbol{\theta}}^{(n)} \text{ and } \mathbf{S}_i^{(n)} = \mathbf{s} \right\}, \quad \mathbf{s} \in \{\boldsymbol{\Gamma}_{\widehat{\boldsymbol{\theta}}^{(n)}} \mathbf{s}_1, \dots, \boldsymbol{\Gamma}_{\widehat{\boldsymbol{\theta}}^{(n)}} \mathbf{s}_{n_S}\}. \quad (4.24)$$

Because of the data-driven choice of $\widehat{\boldsymbol{\theta}}^{(n)}$, the grid $\mathfrak{G}^{(n)}(\widehat{\boldsymbol{\theta}}^{(n)})$ is random. If $n_R \rightarrow \infty$ and $n_S \rightarrow \infty$, the assumptions in Proposition 5 are satisfied a.s., and the Glivenko-Cantelli result (4.20) holds a.s. as well. Similar consistency properties then follow for quantile contours and regions, parallels, and hypermeridians.

4.3 — Distribution-freeness, ancillarity, and equivariance

Denote by $\mathbb{P}_{\mathbf{Z}}^{(n)}$ the joint distribution of the n -tuple $\mathbf{Z}^{(n)} := (\mathbf{Z}_1^{(n)}, \dots, \mathbf{Z}_n^{(n)})$ of i.i.d. observations with common distribution $\mathbb{P}^{\mathbf{Z}} \in \mathfrak{P}_d$ and let $\mathfrak{P}_d^{(n)} := \{\mathbb{P}_{\mathbf{Z}}^{(n)} \mid \mathbb{P}^{\mathbf{Z}} \in \mathfrak{P}_d\}$. Denote by $\mathbf{Z}_{(\cdot)}^{(n)} = (\mathbf{Z}_{(1)}^{(n)}, \dots, \mathbf{Z}_{(n)}^{(n)})$ the *order statistic* of $\mathbf{Z}^{(n)}$, obtained by ordering the observations via some arbitrary criterion, e.g., by increasing values of first components. As in \mathbb{R}^d , the order statistic generates the sigma-field of permutationally invariant measurable functions of $\mathbf{Z}^{(n)}$, and it readily follows from the factorization criterion that it is sufficient for $\mathfrak{P}_d^{(n)}$ (see Proposition 6 below).

It is quite natural, thus, to assume that the estimator $\widehat{\boldsymbol{\theta}}^{(n)}$ is a symmetric function of the $\mathbf{Z}^{(n)}$'s, hence is measurable with respect to $\mathbf{Z}_{(\cdot)}^{(n)}$: were it not, the Rao-Blackwell theorem, indeed, would recommend to replace it with $\mathbb{E}[\widehat{\boldsymbol{\theta}}^{(n)} \mid \mathbf{Z}_{(\cdot)}^{(n)}]$ which, by construction is $\mathbf{Z}_{(\cdot)}^{(n)}$ -measurable. The random grid $\mathfrak{G}^{(n)}(\widehat{\boldsymbol{\theta}}^{(n)})$ then is also $\mathbf{Z}_{(\cdot)}^{(n)}$ -measurable, and so is the n -tuple $(\mathbf{F}^{(n)}(\mathbf{Z}_{(1)}^{(n)}), \dots, \mathbf{F}^{(n)}(\mathbf{Z}_{(n)}^{(n)}))$. The following results extend to the spherical context the essential properties of univariate and multivariate order statistics, ranks, and signs.

Proposition 6 *Let $\{\mathbf{Z}_1^{(n)}, \dots, \mathbf{Z}_n^{(n)}\}$ be i.i.d. with distribution $\mathbb{P}^{\mathbf{Z}} \in \mathfrak{P}_d$. Assume that $\widehat{\boldsymbol{\theta}}_{\mathbf{M}}^{(n)}$ is $\mathbf{Z}_{(\cdot)}^{(n)}$ -measurable. Denote by $\mathbf{F}^{(n)}$ its empirical distribution function, computed as described in Section 4.2. Then, in the notation of Section 4.2,*

- (i) *the order statistic $\mathbf{Z}_{(\cdot)}^{(n)}$ is sufficient and complete, hence minimal sufficient, for $\mathbb{P}^{\mathbf{Z}} \in \mathfrak{P}_d$;*
- (ii) *for all $\mathbb{P}^{\mathbf{Z}} \in \mathfrak{P}_d$, conditional on $\widehat{\boldsymbol{\theta}}^{(n)}$, $\mathbf{F}^{(n)}(\mathbf{Z}^{(n)}) := (\mathbf{F}^{(n)}(\mathbf{Z}_1^{(n)}), \dots, \mathbf{F}^{(n)}(\mathbf{Z}_n^{(n)}))$ is uniformly distributed over the $n!/n_0!$ permutations (with repetitions, $\widehat{\boldsymbol{\theta}}^{(n)}$ being counted as n_0 indistinguishable points in case $n_0 > 1$) of the grid $\mathfrak{G}^{(n)}(\widehat{\boldsymbol{\theta}}^{(n)})$;*
- (iii) *the vector of ranks $\mathbf{R}^{(n)} := (\mathcal{R}_1^{(n)}, \dots, \mathcal{R}_{n_S}^{(n)})$ is distribution-free and uniformly distributed over the $n!/n_0!(n_S!)^{n_R}$ permutations with repetitions of $\{0$ (n_0 copies), 1 (n_S copies), \dots , n_R (n_S copies)); the rank $\mathcal{R}_i^{(n)}$, $i = 1, \dots, n$ takes value 0 with probability n_0/n and value j with probability n_S/n , $j = 1, \dots, n_R$;*
- (iv) *conditionally on $\widehat{\boldsymbol{\theta}}^{(n)}$, the vector of signs $(\mathbf{S}_1^{(n)}, \dots, \mathbf{S}_n^{(n)})$ is uniformly distributed over the $n!/n_0!(n_R!)^{n_S}$ permutations with repetitions of $\{0$ (n_0 copies), $\boldsymbol{\Gamma}_{\widehat{\boldsymbol{\theta}}^{(n)}} \mathbf{s}_1$ (n_R copies), \dots , $\boldsymbol{\Gamma}_{\widehat{\boldsymbol{\theta}}^{(n)}} \mathbf{s}_{n_S}$ (n_R copies));*
- (v) *conditional on $\widehat{\boldsymbol{\theta}}^{(n)}$ and for $n_0 = 0$, the vector of ranks $(\mathcal{R}_1^{(n)}, \dots, \mathcal{R}_n^{(n)})$ and the vector of signs $(\mathbf{S}_1^{(n)}, \dots, \mathbf{S}_n^{(n)})$ are mutually independent for all $\mathbb{P}^{\mathbf{Z}} \in \mathfrak{P}_d$.*

Note that part (v) of this proposition only holds for $n_0 = 0$. For $n_0 > 0$, indeed, $R_i^{(n)} = 0$ automatically implies $S_i^{(n)} = 0$. However, since $n_0/n \rightarrow 0$ as $n \rightarrow \infty$, this dependence between ranks and signs induced by the n_0 observations mapped to $\widehat{\boldsymbol{\theta}}^{(n)}$ is asymptotically negligible. A tie-breaking procedure similar to that proposed in Hallin et al. (2021a) easily allows for removing this restriction; details are skipped.

An essential property of traditional (univariate) ranks and the center-outward ranks and signs introduced in Hallin et al. (2021a) is their *maximal ancillarity*, which is the source of their success in inferential problems. It follows from Proposition 6 that, due to the dependence on $\widehat{\boldsymbol{\theta}}^{(n)}$ of the signs $S_i^{(n)}$, this property cannot hold for the directional ranks and signs defined in (4.22) and (4.21). However, defining $\bar{S}_i^{(n)} := \Gamma_{\widehat{\boldsymbol{\theta}}^{(n)}}^\top S_i^{(n)}$ $i = 1, \dots, n$, with values in $\mathfrak{S}^{(ns)}$ (in $\{0\} \cup \mathfrak{S}^{(ns)}$ if $n_0 > 0$), we recover this highly desirable property: call $\bar{S}_i^{(n)}$ the *absolute sign* of $Z_i^{(n)}$. Absolute signs are slightly less informative than the signs; actually, they characterize the signs up to an orthogonal transformation of the equatorial hypersphere—i.e., up to the (arbitrary) choice of an orthonormal coordinate system (the columns of $\Gamma_{\widehat{\boldsymbol{\theta}}^{(n)}}$) for the equatorial hyperplane defined by $\widehat{\boldsymbol{\theta}}^{(n)}$. In particular, all cosines of the form $(S_i^{(n)})^\top S_j^{(n)}$ are preserved in the transformation from signs to absolute signs:

$$(S_i^{(n)})^\top S_j^{(n)} = (\bar{S}_i^{(n)})^\top \bar{S}_j^{(n)} \quad i, j = 1, \dots, n. \quad (4.25)$$

Proposition 7 Under the assumptions of Proposition 6,

- (i) the vector of absolute signs $(\bar{S}_1^{(n)}, \dots, \bar{S}_n^{(n)})$ is distribution-free under $\mathfrak{F}_d^{(n)}$ and uniformly distributed over the $n!/n_0!(n_R!)^{ns}$ permutations with repetitions of $\{0$ (n_0 copies), s_1 (n_R copies), \dots , s_{n_S} (n_R copies) $\}$;
- (ii) for $n_0 = 0$, the vector of ranks $(R_1^{(n)}, \dots, R_n^{(n)})$ and the vector $(\bar{S}_1^{(n)}, \dots, \bar{S}_n^{(n)})$ of absolute signs are mutually independent for all $P^Z \in \mathfrak{F}_d$;
- (iii) the σ -field generated by the ranks $R_1^{(n)}, \dots, R_n^{(n)}$ and the absolute signs $\bar{S}_1^{(n)}, \dots, \bar{S}_n^{(n)}$ is maximal ancillary for the family of distributions $\mathfrak{F}_d^{(n)}$.

Here again, the restriction of point (ii) to $n_0 = 0$ can be waived via the tie-breaking procedure described in Hallin et al. (2021a).

The importance of absolute signs is of a theoretical nature and stems from the maximal ancillarity property (Proposition 7 (iii)). They seldom are needed in practice, where either a coordinate system of the parallel/meridian type is to be constructed—in which case the signs as defined in (4.21) are fine—or distribution-free tests are to be performed, which typically are based on quadratic test statistics involving signs via scalar products of the form (4.25) only, hence do not depend on the type of signs adopted.

Equivariance and invariance properties with respect to orthogonal transformations play a crucial role in directional statistics. The following proposition provides invariance/equivariance properties of the empirical distribution functions, signs, and ranks.

Proposition 8 Denote by $\mathfrak{G}^{(n)}$ an n -point grid and by $\mathbf{z} := (z_1, \dots, z_n)$ an arbitrary n -tuple of points on S^{d-1} , by \mathbf{O} a $d \times d$ orthogonal matrix, and by $F_{\mathbf{Oz}}^{(n)}$ the empirical distribution function constructed from $\mathbf{Oz} := (\mathbf{Oz}_1, \dots, \mathbf{Oz}_n)$ and the grid $\mathfrak{G}^{(n)}$ as described in Section 4.2. Assume that $\widehat{\boldsymbol{\theta}}^{(n)}$ is such that $\widehat{\boldsymbol{\theta}}^{(n)}(\mathbf{Oz}) = \mathbf{O}\widehat{\boldsymbol{\theta}}^{(n)}(\mathbf{z})$. Then,

- (i) $F_{\mathbf{Oz}}^{(n)}(\mathbf{Oz}_i) = \mathbf{O}F_{\mathbf{z}}^{(n)}(\mathbf{z}_i)$, $i = 1, \dots, n$;
- (ii) denoting by $R_{\mathbf{Oz}}^{(n)}(\mathbf{Oz}_i)$ and $\bar{S}_{\mathbf{Oz}}^{(n)}(\mathbf{Oz}_i)$, respectively, the rank and the absolute sign of \mathbf{Oz}_i computed from $F_{\mathbf{Oz}}^{(n)}(\mathbf{Oz}_i)$,

$$R_{\mathbf{Oz}}^{(n)}(\mathbf{Oz}_i) = R_{\mathbf{z}}^{(n)}(\mathbf{z}_i) \quad \text{and} \quad \bar{S}_{\mathbf{Oz}}^{(n)}(\mathbf{Oz}_i) = \bar{S}_{\mathbf{z}}^{(n)}(\mathbf{z}_i), \quad i = 1, \dots, n.$$

The empirical directional distribution function thus is equivariant under orthogonal transformations; note that the assumption of orthogonal equivariance property made on $\widehat{\boldsymbol{\theta}}^{(n)}(\mathbf{z})$ is quite natural, and satisfied by all sensible estimators, among which the Fréchet mean and the corresponding $\widehat{\boldsymbol{\theta}}^{(n)}(\mathbf{z})$.

4.4 — Numerical illustration: simulations

To illustrate the concept of quantile contours in (4.23), we generated sequences of $n = 2001$ i.i.d. unit random vectors from three types of distributions on \mathcal{S}^2 :

- (i) the von Mises-Fisher (vMF) distribution (see (1.1)) with concentration $\kappa = 10$ and location $\boldsymbol{\theta} = (0, 0, 1)^\top$. Below, $\mathcal{M}_d(\boldsymbol{\theta}, \kappa)$ denotes the von Mises distribution on \mathcal{S}^{d-1} with location $\boldsymbol{\theta}$ and concentration κ ;
- (ii) the tangent vMF distribution as defined in García-Portugués et al. (2020). The tangent vMF distribution with location $\boldsymbol{\theta}$, angular function G , skewness direction $\boldsymbol{\mu}$, and skewness intensity κ is the distribution of

$$\mathbf{Z} := V\boldsymbol{\theta} + \sqrt{1 - V^2}\boldsymbol{\Gamma}_\theta\mathbf{U}, \quad (4.26)$$

- where $\boldsymbol{\Gamma}_\theta$ is the $d \times (d - 1)$ semi-orthogonal matrix described in Part (2b) of Step 2 of the construction (Section 4.2) of the grid, V (an absolutely continuous scalar random variable) and $\mathbf{U} \sim \mathcal{M}_2(\boldsymbol{\mu}, \kappa)$ are mutually independent; in the simulation, we set $\boldsymbol{\theta} = (0, 0, 1)^\top$, $\boldsymbol{\mu} = (0.7, \sqrt{0.51})^\top$, $\kappa = 10$, and $V = 2\tilde{V} - 1$ with $\tilde{V} \sim \text{Beta}(2, 8)$;
- (iii) a mixture of two vMF distributions—the distribution of $I(U \leq 0.3)\mathbf{Z}_1 + I(U > 0.3)\mathbf{Z}_2$, where $U \sim \text{U}[0, 1]$, $\mathbf{Z}_1 \sim \mathcal{M}_3(\boldsymbol{\theta}_1, \kappa_1)$ and $\mathbf{Z}_2 \sim \mathcal{M}_3(\boldsymbol{\theta}_2, \kappa_2)$ are mutually independent. We set $\kappa_1 = 20$, $\boldsymbol{\theta}_1 = (0, -0.5, \sqrt{0.75})^\top$, $\kappa_2 = 20$ and $\boldsymbol{\theta}_2 = (0, 0.5, \sqrt{0.75})^\top$ in the simulation.

For each simulation scheme, we computed the Fréchet mean via the `rbase.robust` function from the R package `RiemBase`. The optimal coupling between the sample points and the regular grid has been obtained by using the fast network simplex algorithm of Bonneel et al. (2011) as implemented in the `transport` function of the R package `transport`. We factorized $n = n_R n_S + n_0$ with $n_R = 40$, $n_S = 50$ and $n_0 = 1$. Hence each empirical quantile contour consists in 50 points. Plots of the median $\widehat{\boldsymbol{\theta}}^{(n)}$, the empirical quantile contours for probability contents 12.2% (rank = 5), 48.8% (rank = 20), and 70.7% (rank = 29) are shown in Figures 3 (left, middle, and right panels for the simulation schemes (i), (ii), and (iii), respectively). We also provide in the same figures the corresponding empirical meridians (points with the same color on the figures have the same signs).

Under the vMF distribution (Figure 3, left panel), the empirical quantile contours are symmetrically distributed around the median, as expected from the rotational symmetry of the vMF distribution. Under the mixture distribution (Figure 3, middle panel), quantile contours adapt to the underlying multimodality, and the median is located in the mixture component with larger probability weight. Under the tangent vMF distribution, where skewness is involved (Figure 3, right panel), the empirical quantile contours exhibit a distinctive skewed shape. Our empirical quantile contours thus nicely pick up the shapes of the underlying distributions while controlling the probability contents of the corresponding quantile regions.

5 — APPLICATIONS: DIRECTIONAL GOODNESS-OF-FIT

Classical goodness-of-fit tests (Kolmogorov-Smirnov, Cramér-von Mises, etc.) are based on distances between distribution functions. Our concepts of population and empirical directional distribution functions quite naturally lead to the construction of directional versions based on distances between $\mathbf{F}^{(n)}$ and \mathbf{F} . Assuming that a sample of i.i.d.

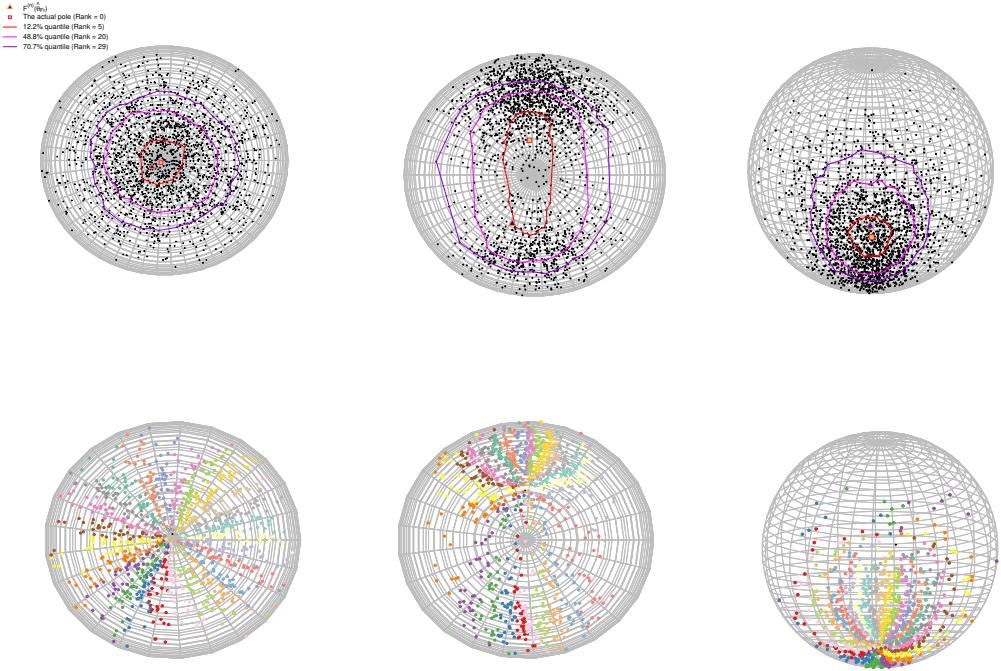


FIGURE 3 Upper panel: empirical quantile contours (probability contents 12.2%, 48.8%, and 70.7%, respectively) computed from $n = 2001$ ($n_R = 40$, $n_S = 50$ and $n_0 = 1$) points drawn from a von Mises-Fisher distribution (left), a mixture of two von Mises-Fisher distributions (middle) and a tangent von Mises-Fisher distribution (right). Lower panel: the corresponding empirical meridians; points with the same color have the same signs.

random unit vectors $\mathbf{Z}_1^{(n)}, \dots, \mathbf{Z}_n^{(n)}$ have common distribution $\mathbf{P}^{\mathbf{Z}}$ the goodness-of-fit problem consists in testing the null hypothesis $\mathcal{H}_0 : \mathbf{P}^{\mathbf{Z}} = \mathbf{P}_0$ against $\mathcal{H}_1 : \mathbf{P}^{\mathbf{Z}} \neq \mathbf{P}_0$, where \mathbf{P}_0 is some specified distribution. This has been studied extensively in directional statistics, with special attention to the problem of testing uniformity—in which case \mathbf{P}_0 is the uniform distribution $\mathbf{P}^{\mathbf{U}}$ over \mathcal{S}^{d-1} . In view of Proposition 3, testing $\mathcal{H}_0 : \mathbf{P}^{\mathbf{Z}} = \mathbf{P}_0$ against $\mathcal{H}_1 : \mathbf{P}^{\mathbf{Z}} \neq \mathbf{P}_0$ is equivalent to testing $\mathcal{H}_0 : \mathbf{F} = \mathbf{F}_0$ against $\mathcal{H}_1 : \mathbf{F} \neq \mathbf{F}_0$ where \mathbf{F}_0 denotes the distribution function of \mathbf{P}_0 —i.e., $\mathbf{F}_0(\mathbf{z}) = \mathbf{z}$ in case $\mathbf{P}_0 = \mathbf{P}^{\mathbf{U}}$.

The test we are proposing in this Section is a Cramér-von Mises-type test that rejects the null hypothesis for large values of the test statistic

$$T_n := n^{-1} \sum_{i=1}^n \left\| \mathbf{F}^{(n)}(\mathbf{Z}_i^{(n)}) - \mathbf{F}_0(\mathbf{Z}_i^{(n)}) \right\|^2, \quad (5.27)$$

where $\mathbf{F}^{(n)}$ is obtained as in Section 4 (the construction considered in Section 4.1 here is sufficient). That test statistic is the empirical counterpart of the (squared) L_2 distance $\mathbb{E} \left[\left\| \mathbf{F}(\mathbf{Z}_i^{(n)}) - \mathbf{F}_0(\mathbf{Z}_i^{(n)}) \right\|^2 \right]$. As always in goodness-of-fit tests, the critical value c_α such that $\mathbb{P}[T_n > c_\alpha] = \alpha$ under \mathcal{H}_0 is easily approximated via Monte Carlo simulations since the

null hypothesis is simple; the resulting test has exact size α . The following result establishes its consistency.

Proposition 9 Assume that $\mathbf{Z}_1^{(n)}, \dots, \mathbf{Z}_n^{(n)}$ are i.i.d. with common optimal transport map \mathbf{F} . Then, provided that the uniform discrete distribution over the n -points grid $\mathfrak{G}^{(n)}$ converges weakly, as $n \rightarrow \infty$, to the uniform distribution \mathbb{P}^U over \mathcal{S}^{d-1} ,

- (i) $T_n = o_{\mathbb{P}}(1)$ as $n \rightarrow \infty$ under \mathcal{H}_0 , while
- (ii) T_n converges in probability to a strictly positive constant as $n \rightarrow \infty$ if $\mathbf{F} \neq \mathbf{F}_0$.

It follows from Proposition 9 that the test ϕ_n is asymptotically consistent against any fixed alternative and therefore qualifies as a universally consistent omnibus test.

In order to investigate the finite-sample performances of our test of uniformity based on (5.27), we performed Monte Carlo size and power comparisons of our test and the projected Cramér-Von Mises (PCvM), projected Anderson-Darling (PAD), and projected Rothman (PRt) tests recently proposed in García-Portugués et al. (2022). To do so, we generated $N = 1000$ independent samples of $n = 400$ i.i.d. unit random vectors with various distributions:

- (i) the uniform distribution;
- (ii) vMF distributions, all with location parameter $\boldsymbol{\theta} = (0, 0, 1)^\top$, with various concentration parameters $\kappa = 0.05$, $\kappa = 0.1$, and $\kappa = 0.5$;
- (iii) tangent vMF distributions as in (4.26), all with angular distribution F_* , location $\boldsymbol{\theta} = (0, 0, 1)^\top$, and skewness direction $\boldsymbol{\mu} = (0, 1)^\top$, with various skewness intensities $\kappa = 0.05$, $\kappa = 0.1$, and $\kappa = 0.5$;
- (iv) mixtures of two vMFs, of the form $I(U \leq 0.5)\mathbf{Z}_1 + I(U > 0.5)\mathbf{Z}_2$, where $U \sim U[0, 1]$, $\mathbf{Z}_1 \sim \mathcal{M}_3(\boldsymbol{\theta}_1, \kappa_1)$, and $\mathbf{Z}_2 \sim \mathcal{M}_3(\boldsymbol{\theta}_2, \kappa_2)$ are mutually independent, with $\boldsymbol{\theta}_1 = (0, -0.3, \sqrt{0.91})^\top$ and $\boldsymbol{\theta}_2 = (0.3, \sqrt{0.66}, 0.5)^\top$, and various concentration parameters $\kappa_1 = \kappa_2 = 0.067$, $\kappa_1 = \kappa_2 = 0.1$, and $\kappa_1 = \kappa_2 = 0.2$;
- (v) mixtures of two vMFs and a tangent vMF of the form $I(U \leq 0.5)\mathbf{Z}_1 + I(0.5 < U < 0.75)\mathbf{Z}_2 + I(U \geq 0.75)\mathbf{Z}_3$, where $U \sim U[0, 1]$, \mathbf{Z}_1 , \mathbf{Z}_2 and \mathbf{Z}_3 are mutually independent. The mixture component \mathbf{Z}_1 follows the tangent vMF distribution as in scheme (iii) with various skewness intensities $\kappa_1 = 0.1$, $\kappa_1 = 0.2$ and $\kappa_1 = 0.33$,

TABLE 1 Rejection frequencies of the OT, PCvM, PAD and PRt tests of uniformity over \mathcal{S}^2 under the uniform, vMF, tangent vMF, mixtures of two vMF distributions and mixtures of two vMFs and a tangent vMF, with various values of concentration or intensity parameter (simulation settings: $N = 1000$ replications and sample size $n = 400$)

	OT	PCvM	PAD	PRt
Uniform	0.050	0.057	0.060	0.056
vMF ($\kappa = 0.05$)	0.070	0.067	0.068	0.067
vMF ($\kappa = 0.1$)	0.135	0.144	0.145	0.142
vMF ($\kappa = 0.5$)	0.996	0.999	0.999	1.000
tangent vMF ($\kappa = 0.05$)	0.106	0.081	0.084	0.078
tangent vMF ($\kappa = 0.1$)	0.230	0.172	0.166	0.170
tangent vMF ($\kappa = 0.5$)	0.680	0.598	0.592	0.605
Mixture of two vMFs ($\kappa_1 = \kappa_2 = 0.067$)	0.074	0.073	0.074	0.072
Mixture of two vMFs ($\kappa_1 = \kappa_2 = 0.1$)	0.119	0.097	0.099	0.094
Mixture of two vMFs ($\kappa_1 = \kappa_2 = 0.2$)	0.322	0.310	0.307	0.306
Mixture of two vMFs and a tangent vMF ($\kappa_1 = \kappa_2 = \kappa_3 = 0.1$)	0.189	0.120	0.122	0.116
Mixture of two vMFs and a tangent vMF ($\kappa_1 = \kappa_2 = \kappa_3 = 0.2$)	0.456	0.333	0.325	0.333
Mixture of two vMFs and a tangent vMF ($\kappa_1 = \kappa_2 = \kappa_3 = 0.33$)	0.857	0.782	0.776	0.780

and $\mathbf{Z}_2 \sim \mathcal{M}_p(\boldsymbol{\theta}_2, \kappa_2)$ and $\mathbf{Z}_3 \sim \mathcal{M}_p(\boldsymbol{\theta}_3, \kappa_3)$ as in scheme (iv) with concentration parameters $\kappa_2 = \kappa_3 = 0.1$, $\kappa_2 = \kappa_3 = 0.2$; and $\kappa_2 = \kappa_3 = 0.33$.

In Table 1, we report the rejection frequencies (at nominal level $\alpha = 0.05$), out of $N = 1000$ replications, of the optimal transport Cramér-Von Mises test described in (5.27) (OT), the projected Cramér-Von Mises test (PCvM), the projected Anderson-Darling test (PAD), and the projected Rothman test (PRt) of uniformity. The critical values are obtained through 2000 Monte Carlo replications. Inspection of Table 1 reveals that all rejection frequencies under the null hypothesis of a uniform distribution are close to the nominal level 0.05. Under the vMF distributions, all tests show similar performances. However, under non-rotationally symmetric alternatives such as the tangent vMF or mixture distributions, our test uniformly outperforms all its competitors.

6 — APPLICATIONS: DIRECTIONAL MANOVA

Let $\mathbf{X}_{i1}^{(n_i)}, \dots, \mathbf{X}_{in_i}^{(n_i)}, i = 1, \dots, m$, denote $m (\geq 2)$ independent samples on the unit hypersphere S^{d-1} . For each i , we assume that $\mathbf{X}_{i1}^{(n_i)}, \dots, \mathbf{X}_{in_i}^{(n_i)}$ are i.i.d. with common distribution P_i (absolutely continuous with density f_i) and directional distribution $\mathbf{F}_i, i = 1, \dots, m$. The problem of interest is to test the null hypothesis $\mathcal{H}_0 : \mathbf{F}_1 = \dots = \mathbf{F}_m =: \mathbf{F}$ (unspecified \mathbf{F}) of no treatment effect.

Let $\mathbf{F}^{(n)}$ denote the empirical directional distribution function computed from the pooled sample

$$\{\mathbf{Y}_1^{(n)}, \dots, \mathbf{Y}_n^{(n)}\} := \{\mathbf{X}_{11}^{(n_1)}, \dots, \mathbf{X}_{1n_1}^{(n_1)}, \dots, \mathbf{X}_{m1}^{(n_m)}, \dots, \mathbf{X}_{mn_m}^{(n_m)}\}.$$

The tests we propose here are based on $\Delta_{\mathbf{J}}^{(n)} := (\Delta_{1;\mathbf{J}}^{(n_1)'}, \dots, \Delta_{m;\mathbf{J}}^{(n_m)'})'$ where, for some score function $\mathbf{J} : S^{d-1} \rightarrow \mathbb{R}^{\bar{d}}$,

$$\Delta_{i;\mathbf{J}}^{(n_i)} := n_i^{-1/2} \sum_{j=1}^{n_i} \mathbf{J}(\mathbf{F}^{(n)}(\mathbf{X}_{ij}^{(n_i)})) - n^{-1/2} \sum_{\ell=1}^n \frac{n_i^{1/2}}{n^{1/2}} \mathbf{J}(\mathbf{F}^{(n)}(\mathbf{Y}_{\ell}^{(n)})) = n^{-1/2} \sum_{\ell=1}^n (\mathbf{a}_{i\ell}^{(n)} - \bar{\mathbf{a}}_i^{(n)}) \mathbf{J}(\mathbf{F}^{(n)}(\mathbf{Y}_{\ell}^{(n)})), \quad i = 1, \dots, m$$

with $\mathbf{a}_{i\ell}^{(n)} := n^{1/2}/n_i^{1/2} \mathbb{1}_{(n_1+\dots+n_{i-1}+1 \leq \ell \leq n_1+\dots+n_{i-1}+n_i)}$ and $\bar{\mathbf{a}}_i^{(n)} = n^{-1} \sum_{\ell=1}^n \mathbf{a}_{i\ell}^{(n)} = n_i^{1/2}/n^{1/2} \mathbb{1}_{(\cdot)}$ denoting the indicator function). Below we assume that $r_i^{(n)} := n_i/n$ converges to a constant r_i as $n \rightarrow \infty$. Letting $\mathbf{D}_{\mathbf{J}} := \text{Var}(\mathbf{J}(\mathbf{U}))$ where \mathbf{U} is uniform over S^{d-1} , our tests reject \mathcal{H}_0 for large values of $Q_{\mathbf{J}}^{(n)} := \Delta_{\mathbf{J}}^{(n)'} (\mathbf{I}_m \otimes \mathbf{D}_{\mathbf{J}}^{-}) \Delta_{\mathbf{J}}^{(n)}$, where $\mathbf{D}_{\mathbf{J}}^{-}$ denotes the Moore-Penrose inverse of $\mathbf{D}_{\mathbf{J}}$. The next result shows that $Q_{\mathbf{J}}^{(n)}$ is asymptotically chi-square under \mathcal{H}_0 and some mild regularity assumptions on the score function \mathbf{J} .

Proposition 10 *Assume that (i) \mathbf{J} is continuous over S^{d-1} and (ii) \mathbf{J} is square-integrable, that is, $\int_{S^{d-1}} \|\mathbf{J}(\mathbf{u})\|^2 d\mathbf{P}^{\mathbf{U}}(\mathbf{u}) < \infty$, and, (iii) for any sequence $\mathfrak{G}^{(n)} := \{\mathfrak{G}_1^{(n)}, \dots, \mathfrak{G}_n^{(n)}\}$ of n -tuples in S^{d-1} such that the uniform discrete distribution over $\mathfrak{G}^{(n)}$ converges weakly to $\mathbf{P}^{\mathbf{U}}$ as $n \rightarrow \infty$, $\lim_{n \rightarrow \infty} n^{-1} \sum_{\ell=1}^n \|\mathbf{J}(\mathfrak{G}_{\ell}^{(n)})\|^2 = \int_{S^{d-1}} \|\mathbf{J}(\mathbf{u})\|^2 d\mathbf{P}^{\mathbf{U}}(\mathbf{u})$. Then, as $n \rightarrow \infty$, $Q_{\mathbf{J}}^{(n)}$ under \mathcal{H}_0 is asymptotically chi-square with $(m-1)d^*$ degrees of freedom, where d^* is the rank of the matrix $\mathbf{D}_{\mathbf{J}}$.*

The MANOVA tests we propose reject the hypothesis of no treatment effect at asymptotic level α whenever $Q_{\mathbf{J}}^{(n)}$ exceeds $\chi_{(m-1)d^*; 1-\alpha}^2$, where $\chi_{p;\tau}^2$ stands for the quantile of order τ of a chi-square distribution with p degrees of freedom.

These tests are fully distribution-free. Below, we investigate their finite-sample performance for several scores:

- (i) the uniform score $\mathbf{J}(\mathbf{u}) := \mathbf{u}$;
- (ii) the estimated vMF-location score $\mathbf{J}(\mathbf{F}^{(n)}(\mathbf{Y}_{\ell}^{(n)})) := \hat{\kappa} \sqrt{1 - \left(G_{\hat{\kappa}}^{-1} \left(1 - \frac{R_{\ell}^{(n)}}{nR+1}\right)\right)^2} \mathbf{S}_{\ell}^{(n)}$, where $\hat{\kappa}$ is the vMF maximum-likelihood estimator of the concentration parameter, G_{κ} is the distribution function of $\mathbf{Z}'\boldsymbol{\theta}$ with $\mathbf{Z} \sim \mathcal{M}_d(\boldsymbol{\theta}, \kappa)$,

$R_\ell^{(n)} := R^{(n)}(\mathbf{Y}_\ell^{(n)}) = (n_R + 1) \left[1 - F_*((\mathbf{F}^{(n)}(\mathbf{Y}_\ell^{(n)}))' \hat{\boldsymbol{\theta}}^{(n)}) \right]$, $\mathbf{S}_\ell^{(n)} := \mathbf{S}_{\hat{\boldsymbol{\theta}}^{(n)}}(\mathbf{F}^{(n)}(\mathbf{Y}_\ell^{(n)}))$, and $\hat{\boldsymbol{\theta}}^{(n)}$ is obtained as in step 1 of the construction of the grid in Section 4.2;

(iii) the estimated vMF-concentration score $\mathbf{J}(\mathbf{F}^{(n)}(\mathbf{Y}_\ell^{(n)})) := G_\kappa^{-1} \left(1 - \frac{R_\ell^{(n)}}{n_R + 1} \right)$, and

(iv) the estimated vMF-location-concentration score (a linear combination of the scores in (ii) and (iii))

$$\mathbf{J}(\mathbf{F}^{(n)}(\mathbf{Y}_\ell^{(n)})) := \hat{\kappa} \left\{ G_\kappa^{-1} \left(1 - \frac{R_\ell^{(n)}}{n_R + 1} \right) \hat{\boldsymbol{\theta}}^{(n)} + \sqrt{1 - \left(G_\kappa^{-1} \left(1 - \frac{R_\ell^{(n)}}{n_R + 1} \right) \right)^2} \mathbf{S}_\ell^{(n)} \right\}.$$

In the simulation exercise below, we compare the resulting tests with their pseudo-vMF (pvMF) counterpart, which rejects the null hypothesis at asymptotic level α whenever $Q^{(n)} > \chi_{(m-1)(d-1); 1-\alpha}^2$, where

$$Q^{(n)} := (d-1) \left(\sum_{i=1}^m \frac{n_i D_i}{E_i} (\bar{\mathbf{X}}_i^{(n_i)})' (\mathbf{I}_d - \hat{\boldsymbol{\theta}} \hat{\boldsymbol{\theta}}') \bar{\mathbf{X}}_i^{(n_i)} - \sum_{i,j}^m \frac{n_i n_j}{n} \frac{D_i D_j}{H} (\bar{\mathbf{X}}_i^{(n_i)})' (\mathbf{I}_d - \hat{\boldsymbol{\theta}} \hat{\boldsymbol{\theta}}') \bar{\mathbf{X}}_j^{(n_j)} \right),$$

with $\hat{\boldsymbol{\theta}}$ the sample Fréchet mean, $\bar{\mathbf{X}}_i^{(n_i)} := n_i^{-1} \sum_{j=1}^{n_i} \mathbf{X}_{ij}^{(n_i)}$, $E_i := n_i^{-1} \sum_{j=1}^{n_i} (\mathbf{X}_{ij}^{(n_i)})' \hat{\boldsymbol{\theta}}$, $H := \sum_{i=1}^m r_i^{(n)} D_i^2 B_i$, $D_i := E_i / B_i$, and $B_i := 1 - n_i^{-1} \sum_{j=1}^{n_i} ((\mathbf{X}_{ij}^{(n_i)})' \hat{\boldsymbol{\theta}})^2$; see Ley et al. (2017) for details.

In the Monte-Carlo simulation, we set $d = 3$, $m = 2$, $n_1 = 500$, $n_2 = 600$, hence $n = 1100$. The structured regular grid for the computation of the vMF-location, vMF-concentration, and vMF-location-concentration scores was based on $n_R = 44$, $n_S = 25$, and $n_0 = 0$. The following data-generating processes were considered.

Case (1) (location alternatives): $\mathbf{X}_{1j}^{(n_1)} \sim \mathcal{M}_d(\boldsymbol{\theta}, \kappa)$, $j = 1, \dots, n_1$ and $\mathbf{X}_{2\ell}^{(n_2)} \sim \mathcal{M}_d(\mathbf{O}_\xi \boldsymbol{\theta}, \kappa)$, $\ell = 1, \dots, n_2$ where $\kappa = 3$,

$$\boldsymbol{\theta} = \begin{pmatrix} 1 \\ 0 \\ 0 \end{pmatrix}, \quad \text{and} \quad \mathbf{O}_\xi = \begin{pmatrix} \cos(\pi\xi/15) & -\sin(\pi\xi/15) & 0 \\ \sin(\pi\xi/15) & \cos(\pi\xi/15) & 0 \\ 0 & 0 & 1 \end{pmatrix} \quad \text{with } \xi = 0, 0.2, 0.4, 0.6, 0.8; \quad (6.28)$$

Case (2) (concentration alternatives): $\mathbf{X}_{1j}^{(n_1)} \sim \mathcal{M}_d(\boldsymbol{\theta}, \kappa)$, $j = 1, \dots, n_1$ and $\mathbf{X}_{2\ell}^{(n_2)} \sim \mathcal{M}_d(\boldsymbol{\theta}, \xi + \kappa)$, $\ell = 1, \dots, n_2$ where $\kappa = 3$ and $\boldsymbol{\theta} = (1, 0, 0)'$, with $\xi = 0, 0.5, 1, 1.5, 2$;

Case (3) (multimodal distribution): $\mathbf{X}_{1j}^{(n_1)}$, $j = 1, \dots, n_1$, is a mixture, with mixing probabilities $\frac{3}{8}$, $\frac{3}{8}$, and $\frac{1}{4}$, of $\mathcal{M}_d(\boldsymbol{\theta}_1, \kappa_1)$, $\mathcal{M}_d(\boldsymbol{\theta}_2, \kappa_2)$, and $\mathcal{M}_d(\boldsymbol{\theta}_3, \kappa_3)$, where $\boldsymbol{\theta}_1 = (1, 0, 0)'$, $\kappa_1 = 3$, $\boldsymbol{\theta}_2 = (-0.8, 0.3, \sqrt{0.27})'$, $\kappa_2 = 2$, $\boldsymbol{\theta}_3 = (0, -0.7, \sqrt{0.51})'$, $\kappa_3 = 3$, and $\mathbf{X}_{2\ell}^{(n_2)} = \mathbf{O}_\xi \mathbf{Z}_\ell^{(n_2)}$, $\ell = 1, \dots, n_2$, where $\mathbf{Z}_\ell^{(n_2)}$ has the same distribution as $\mathbf{X}_{1j}^{(n_1)}$ and \mathbf{O}_ξ is as in (6.28) with $\xi = 0, 1, \dots, 5$;

Case (4) (skewed distribution): $\mathbf{X}_{1j}^{(n_1)}$, $j = 1, \dots, n_1$ and $\mathbf{X}_{1j\ell}^{(n_2)}$, $\ell = 1, \dots, n_1$ are generated from a tangent vMF distribution of the form (4.26) with $\boldsymbol{\theta} = (0, 0, 1)'$, $\boldsymbol{\mu} = (0.7, \sqrt{0.51})'$, $\kappa = 1$, with $\tilde{V} \sim \text{Beta}(2, 5)$ for $\mathbf{X}_{1j}^{(n_1)}$ and $\tilde{V} \sim \text{Beta}(2, 5 + \xi)$, $\xi = 0, 0.2, \dots, 1$ for $\mathbf{X}_{2\ell}^{(n_2)}$.

For each case, the experiments were repeated 500 times for the directional rank-based tests and the pvMF test at 0.05 nominal level, for the various values of ξ (where $\xi = 0$ yields \mathcal{H}_0). Figure 4 shows the rejection frequencies of these tests against ξ for Cases (1)–(4). In terms of size ($\xi = 0$), all directional rank-based tests yield rejection rates close to the nominal level while the pvMF test exhibits a severe over-rejection frequency of 0.122 under Case (3), revealing a poor behavior under multi-modality. In terms of power, for the vMF location problem (Case (1)), the vMF-location score, uniform score and vMF-location-concentration score rank-based tests all have rejection rates very close to the pvMF test which is the optimal test in this case. For the vMF-concentration parameter problem (Case (2)), the pvMF test has no power and is outperformed by all the directional rank-based tests, the power of which increases with ξ . For the mixture of three vMF distributions (Case (3)), the rejection rates of the pvMF test under the alternative are meaningless in view of its size problem; the uniform, vMF-location, and vMF-location-concentration score rank-based

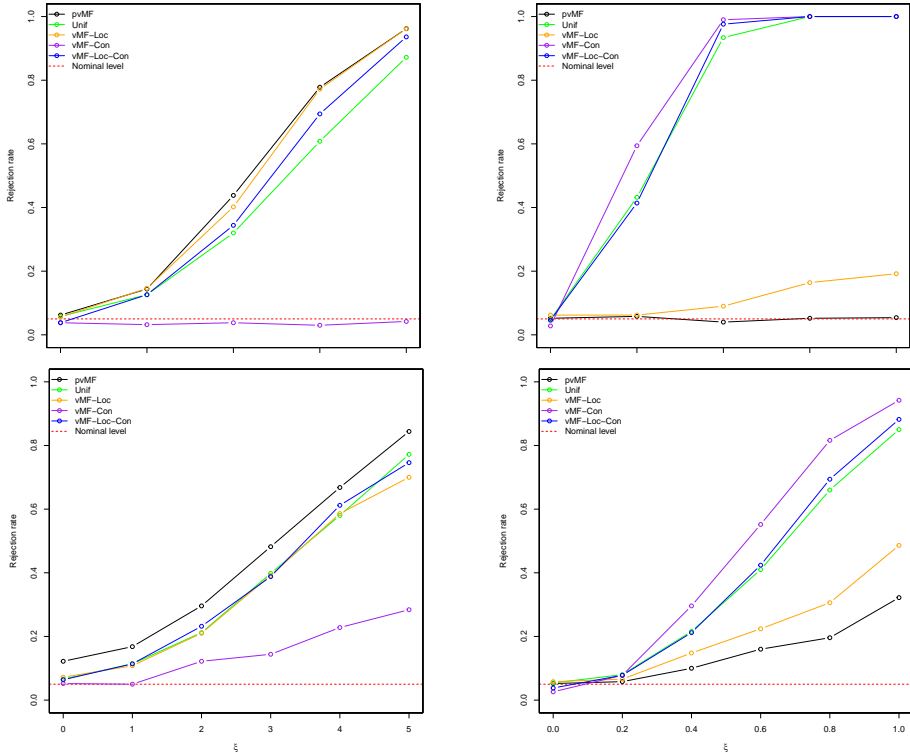


FIGURE 4 The rejection rates (at 0.05 nominal level) of the pseudo-vMF and rank-based tests with uniform, vMF-location, vMF-concentration, and vMF-location-concentration scores, for Cases (1) (top-left panel), (2) (top-right panel), (3) (bottom-left panel), and (4) (bottom-right panel).

tests have greater power than the vMF-concentration score one. When skewness is present (Case (4)), all the rank-based tests outperform the classical pvMF test. In general, the superiority of the vMF-location-concentration score and uniform score rank-based tests is clear, considering their consistency, great power under multi-modality, skewness and vMF distributions (for both the change of the location and concentration parameters). Due to its simplicity, the uniform score is a good choice in terms of computational efficiency.

7 — APPLICATIONS: TWO REAL DATA EXAMPLES

7.1 — MANOVA for Sunspots data

Sunspots are regions on the Sun's photosphere that are darker and cooler than the surrounding areas. They are caused by concentrations of magnetic flux that inhibit convection and are temporary phenomena that experience continuous changes, lasting for hours to days. Their population first increases rapidly and then decreases slowly over a period of approximately 11 years, which is referred to as *solar cycle*. Early in a solar cycle, sunspots appear at higher latitudes and then move towards the equator as the cycle approaches maximum, a phenomenon known as *Spörer's law*. Sunspots are widely used to study and measure solar activity, whose effects may affect earth's long-term climate (Haigh, 2007).

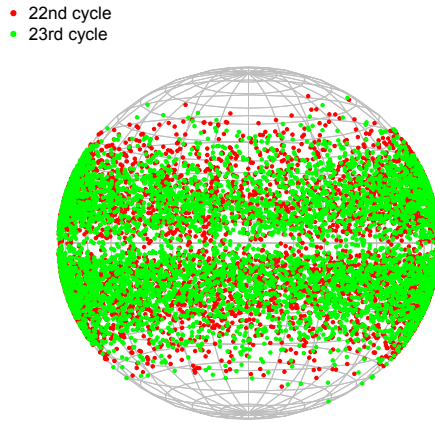


FIGURE 5 Sunspots data: plot of the sunspots of the 22nd solar cycle ($n_1 = 4551$ red points) and the 23rd ($n_2 = 5373$ green points) solar cycle.

pvMF	Unif	vMF-location	vMF-concentration	vMF-location-concentration
0.140	0.036	0.005	0.052	0.005

TABLE 2 Sunspots data: p -values of the pvMF and directional rank-based tests of the equality of distributions of the sunspots of the 22nd and 23rd solar cycles.

The data we analyze is based on the Debrecen Photoheliographic Data (DPD) sunspot catalogue, which contains locations of sunspots since 1974 and is a continuation of the Greenwich Photoheliographic Results (GPR) catalogue (spanning 1874-1976). The data is available from the R package `rotasym`.

The sunspots of the 22nd (September 1986 to July 1996; $n_1 = 4551$ points, in red) and 23rd (August 1996 to November 2008; $n_2 = 5373$ points, in green) solar cycles are shown in in Figure 5. Visual inspection hardly help decide whether these two samples are from the same distribution or not. According to [García-Portugués et al. \(2020\)](#), various tests suggest rotational symmetry around the north pole for the 23rd cycle while rejecting that hypothesis (p -values smaller than 0.02) for the 22nd cycle.

We performed the pvMF and the directional rank-based tests based on the uniform, vMF-location and vMF-concentration scores described in Section 6 for the null hypothesis of equal distributions in the two samples. For the vMF-location and vMF-concentration scores, we factorize $n = 9924$ into $n_S = 121$, $n_R = 82$, and $n_0 = 2$. The p -values of these tests are shown in Table 2. The pvMF test, with p -value 0.14, does not reject the null of the equality of distributions, even at significance level 0.10. The rank-based test with vMF-concentration scores rejects the same hypothesis at level 0.10, but not at level 0.05. The rank-based tests with uniform, vMF-location and vMF-location-concentration scores, with p -values at most 0.036, all suggest that the two samples have different distributions. This result is in line with the Monte Carlo experiments (see, e.g., Case (4)), where the directional rank-based tests significantly outperform the pvMF test when the underlying distribution are not rotationally symmetric.

- ▲ The actual pole (Rank = 0)
- 12.2% quantile (Rank = 5)
- 24.4% quantile (Rank = 10)
- 36.6% quantile (Rank = 15)

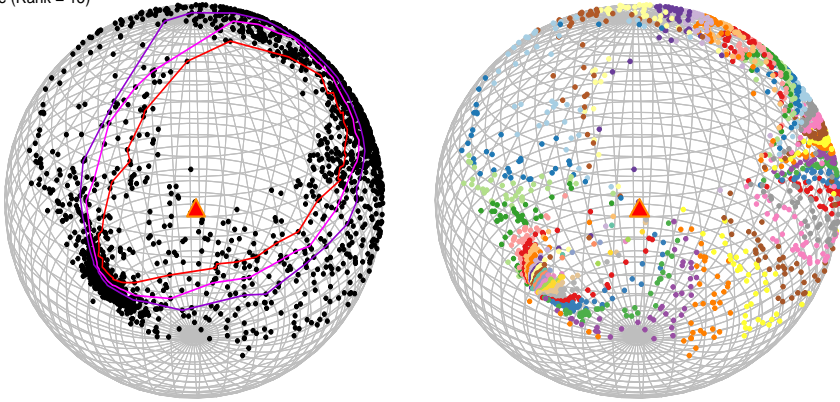


FIGURE 6 Protein data: the empirical quantile contours (probability contents 12.2%, 24.4%, 36.6% respectively) computed from the protein data along with the corresponding empirical meridians ($n_R = 40$, $n_S = 50$ and $n_0 = 1$).

7.2 — Quantile contours for Protein data

Proteins are polypeptide chains built up by amino acids, each of them having a central carbon atom, denoted C_α . Motivated by the key role of C_α atoms in the protein's backbone, [Levitt \(1976\)](#) proposed a representation of the backbone that encodes, from the position of a C_α atom, the location of the next C_α using the pseudo-bond joining them (the term *pseudo* emphasizes that the atoms are not linked by a single chemical bond but rather by several of them). Since the length of pseudo-bonds can be considered constant, the chain of C_α atoms can be represented as a sequence of vectors on the sphere with the parametrization $(\cos(\theta), \sin(\theta) \cos(\tau), \sin(\theta) \sin(\tau))^T$, with $\theta \in [0, \pi)$ and $\tau \in [-\pi, \pi)$, where the origin is set as the previous C_α atom. This codification is employed in the hidden Markov model of [Hamelryck et al. \(2006\)](#). Directional models for evolution of proteins structures have been studied, in particular in [Golden et al. \(2017\)](#). Due to clash-avoiding atom constraints, θ usually lies in $[80^\circ, 150^\circ]$ whereas τ can take any values in $[-180^\circ, 180^\circ)$. In [Figure 6](#), we provide the quantile contours associated with a sample of $n = 2001$ (factorized into $n_R = 40$, $n_S = 50$, and $n_0 = 1$) pseudo-bond directions of the C_α atom. These $n = 2001$ directions have been extracted from the top 500 dataset in [Word et al. \(1999\)](#) by taking $n = 2001$ points randomly within the points for which both θ and τ are available (no missing data). It is evident from the left panel of [Figure 6](#) that the overall distribution of the spherical vectors is highly non-symmetric. Our quantile contours adapt impressively well to this asymmetry.

Acknowledgements

The authors express their warm thanks to Alberto González-Sanz for insightful comments and suggestions on the convergence of empirical transport maps.

references

- Ambrosio, L. and Pratelli, A. (2003) *Existence and Stability Results in the L_1 Theory of Optimal Transportation*, vol. 1813 of *CIME Course, Lecture Notes in Mathematics*. Springer-Verlag Berlin Heidelberg.
- Ameijeiras-Alonso, J., Crujeiras, R. M. and Rodríguez-Casal, A. (2018) Directional statistics for wildfires. In *Applied Directional Statistics* (eds. C. Ley and T. Verdebout), Chapman & Hall/CRC Interdisciplinary Statistics Series, 187–210. Boca Raton: CRC Press.
- del Barrio, E., González-Sanz, A. and Hallin, M. (2022) Nonparametric multiple-output center-outward quantile regression. *arXiv:2204.11756*.
- del Barrio, E., González-Sanz, A. and Loubes, J.-M. (2021) Central limit theorems for general transportation costs. *arXiv:2102.06379*.
- Basu, D. (1959) The family of ancillary statistics. *Sankhyā*, **21**, 247–256.
- Beiglböck, M. (2015) Cyclical monotonicity and the ergodic theorem. *Ergodic Theory Dynam. Systems*, **35**, 710–713.
- Chernozhukov, V., Galichon, A., Hallin, M. and Henry, M. (2017) Monge-Kantorovich depth, quantiles, ranks and signs. *Ann. Statist.*, **45**, 223–256.
- Chikuse, Y. (2003) *Statistics on Special Manifolds*, vol. 174 of *Lecture Notes in Statistics*. Heidelberg: Springer.
- Christie, D. (2015) Efficient von Mises-Fisher concentration parameter estimation using Taylor series. *J. Stat. Comput. Simul.*, **85**, 3259–3265.
- Deb, N., Bhattacharya, B. B. and Sen, B. (2021) Efficiency lower bounds for distribution-free Hotelling-type two-sample tests based on optimal transport. *arXiv:2104.01986v2*.
- Deb, N. and Sen, B. (2022) Multivariate rank-based distribution-free nonparametric testing using measure transportation. *J. Amer. Statist. Assoc.*, to appear.
- Dortet-Bernadet, J.-L. and Wicker, N. (2008) Model-based clustering on the unit sphere with an illustration using gene expression profiles. *Biostatistics*, **9**, 66–80.
- Dryden, I. L. (2005) Statistical analysis on high-dimensional spheres and shape spaces. *Ann. Stat.*, **33**, 1643–1665.
- Gangbo, W. and McCann, R. J. (1996) The geometry of optimal transportation. *Acta Math.*, **177**, 113 – 161. URL: <https://doi.org/10.1007/BF02392620>.
- García-Portugués, E., Barros, A. M. G., Crujeiras, R. M., González-Manteiga, W. and Pereira, J. (2014) A test for directional-linear independence, with applications to wildfire orientation and size. *Stoch. Environ. Res. Risk Assess.*, **28**, 1261–1275.
- García-Portugués, E., Navarro-Esteban, P. and Cuesta-Albertos, J. A. (2022) On a projection-based class of uniformity tests on the hypersphere. *Bernoulli*, to appear.
- García-Portugués, E., Paindaveine, D. and Verdebout, T. (2020) On optimal tests for rotational symmetry against new classes of hyperspherical distributions. *J. Amer. Statist. Assoc.*, **115**, 1873–1887.
- Ghosal, P. and Sen, B. (2022) Multivariate ranks and quantiles using optimal transport: Consistency, rates and nonparametric testing. *Ann. Statist.*, **50**, 1012 – 1037. URL: <https://doi.org/10.1214/21-AOS2136>.
- Golden, M., García-Portugués, E., Sørensen, M., Mardia, K. V., Hamelryck, T. and Hein, J. (2017) A generative angular model of protein structure evolution. *Molecular biology and evolution*, **34**, 2085–2100.
- Haigh, J. D. (2007) The Sun and the Earth's climate. *Living Rev. Sol. Phys.*, **4**, 2.

- Hallin, M. (2022) Measure transportation and statistical decision theory. *Annual Review of Statistics and Its Application*, **9**, 401–424. URL: <https://doi.org/10.1146/annurev-statistics-040220-105948>.
- Hallin, M., del Barrio, E., Cuesta-Albertos, J. A. and Matrán, C. (2021a) Center-outward distribution functions, quantiles, ranks, and signs in \mathbb{R}^d . *Ann. Statist.*, **48**, 1139–1165.
- Hallin, M., Hlubinka, D. and Hudecová, Š. (2022a) Fully distribution-free center-outward rank tests for multiple-output regression and MANOVA. *J. Amer. Statist. Assoc.*, to appear.
- Hallin, M., La Vecchia, D. and Liu, H. (2022b) Center-outward R-estimation for semiparametric VARMA models. *J. Amer. Statist. Assoc.*, **117**.
- (2022c) Rank-based testing for semiparametric var models: a measure transportation approach. *Bernoulli*, **925–938**.
- Hallin, M., Mordant, G. and Segers, J. (2021b) Multivariate goodness-of-fit tests based on Wasserstein distance. *Electron. J. Statist.*, **15**, 1328–1371. URL: <https://doi.org/10.1214/21-EJS1816>.
- Hamelryck, T., Kent, J. T. and Krogh, A. (2006) Sampling realistic protein conformations using local structural bias. *PLoS Comput. Biol.*, **2**, e131.
- Jupp, P. E. and Kume, A. (2020) Measures of goodness of fit obtained by almost-canonical transformations on Riemannian manifolds. *J. Multivar. Anal.*, **176**, 104579.
- Kanika, Kumar, S. and SenGupta, A. (2015) A unified approach to decision-theoretic properties of the MLEs for the mean directions of several Langevin distributions. *J. Multivar. Anal.*, **133**, 160–172.
- Kent, J. T. (1982) The Fisher-Bingham distribution on the sphere. *J. R. Stat. Soc. Ser. B Methodol.*, **44**, 71–80.
- Kent, J. T., Bhattacharjee, S., Hussein, I. I., Faber, W. R. and Jah, M. (2018) Fisher-Bingham-Kent mixture models for angles-only observation processing. In *2018 Space Flight Mechanics Meeting*. Reston: American Institute of Aeronautics and Astronautics.
- Kolouri, S., Park, S. R., Thorpe, M., Slepcev, D. and Rohde, G. K. (2017) Optimal mass transport: Signal processing and machine-learning applications. *IEEE Signal Process. Mag.*, **34**, 43–59.
- Kume, A., Preston, S. P. and Wood, A. T. A. (2013) Saddlepoint approximations for the normalizing constant of Fisher-Bingham distributions on products of spheres and Stiefel manifolds. *Biometrika*, **100**, 971–984.
- Kume, A. and Sei, T. (2018) On the exact maximum likelihood inference of Fisher-Bingham distributions using an adjusted holonomic gradient method. *Stat. Comput.*, **28**, 835–847.
- Levitt, M. (1976) A simplified representation of protein conformations for rapid simulation of protein folding. *J. Mol. Biol.*, **104**, 59–107.
- Ley, C., Sabbah, C. and Verdebout, T. (2014) A new concept of quantiles for directional data and the angular Mahalanobis depth. *Electron. J. Stat.*, **8**, 795–816.
- Ley, C., Swan, Y., Thiam, B. and Verdebout, T. (2013) Optimal R-estimation of a spherical location. *Statist. Sinica*, **23**, 305–332.
- Ley, C., Swan, Y. and Verdebout, T. (2017) Efficient ANOVA for directional data. *Ann. Inst. Statist. Math.*, **69**, 39–62.
- Ley, C. and Verdebout, T. (2017) *Modern Directional Statistics*. Chapman & Hall/CRC Interdisciplinary Statistics Series. Boca Raton: CRC Press.
- Ley, C. and Verdebout, T. (eds.) (2018) *Applied Directional Statistics*. Chapman & Hall/CRC Interdisciplinary Statistics Series. Boca Raton: CRC Press.

- Loeper, G. (2009) On the regularity of solutions of optimal transportation problems. *Acta Math.*, **202**, 241–283.
- Loeper, G. e. (2011) Regularity of optimal maps on the sphere: the quadratic cost and the reflector antenna. *Arch. Ration. Mech. Anal.*, **199**, 269–289.
- Mardia, K. V. and Jupp, P. E. (1999) *Directional Statistics*. Wiley Series in Probability and Statistics. Chichester: Wiley.
- Marinucci, D. and Peccati, G. (2011) *Random Fields on the Sphere*. London Mathematical Society Lecture Note Series. Cambridge: Cambridge University Press.
- Marinucci, D., Pietrobon, D., Balbi, A., Baldi, P., Cabella, P., Kerkycharian, G., Natoli, P., Picard, D. and Vittorio, N. (2008) Spherical needlets for cosmic microwave background data analysis. *Mon. Not. R. Astron. Soc.*, **383**, 539–545.
- McCann, R. (2001) Polar factorization of maps on Riemannian manifolds. *Geom. Funct. Anal.*, **11**, 589–608.
- Paindaveine, D. and Verdebout, T. (2017) Inference on the mode of weak directional signals: a Le Cam perspective on hypothesis testing near singularities. *Ann. Statist.*, **45**, 800–832.
- (2020a) Detecting the direction of a signal on high-dimensional spheres: Non-null and le cam optimality results. *Probab. Theory Relat. Fields*, **176**, 1165–1216.
- (2020b) Inference for spherical location under high concentration. *Ann. Statist.*, **48**, 2982–2998.
- Pratelli, A. (2008) On the sufficiency of c -cyclical monotonicity for optimality of transport plans. *Mathematische Zeitschrift*, **258**, 677–690.
- Rao, J. and SenGupta, A. (2001) *Topics in Circular Statistics*, vol. 5 of *Series on Multivariate Analysis*. Singapore: World Scientific.
- Rudin, W. (1976) *Principles of mathematical analysis*, vol. 3. McGraw-hill New York.
- Rüschendorf, L. (1996) On c -optimal random variables. *Statist. Probab. Lett.*, **27**, 267–270. URL: <https://EconPapers.repec.org/RePEc:eee:stapro:v:27:y:1996:i:3:p:267-270>.
- Sealy, J. L. and Wood, A. T. A. (2019) Scaled von Mises–Fisher distributions and regression models for paleomagnetic directional data. *J. Amer. Statist. Assoc.*, **114**, 1547–1560.
- Schachermayer, W. and Teichmann, J. (2008) Characterization of optimal transport plans for the Monge-Kantotovich problem. *Proc. Amer. Math. Soc.*, **137**, 519–529.
- Shi, H., Drton, M. and Han, F. (2022a) Distribution-free consistent independence tests via center-outward ranks and signs. *J. Amer. Statist. Assoc.*, to appear. URL: <https://doi.org/10.1080/01621459.2020.1782223>.
- Shi, H., Hallin, M., Drton, M. and Han, F. (2022b) On universally consistent and fully distribution-free rank tests of vector independence. *Ann. Statist.*, **50**, 1933–1959.
- Shorack, G. (2000) *Probability for Statisticians*. Springer.
- Torous, W., Gunsilius, F. and Rigollet, P. (2022) An optimal transport approach to causal inference. *arXiv:2108.05858*.
- Verdebout, T. (2017) On the efficiency of some rank-based test for the homogeneity of concentrations. *J. Stat. Plann. Inference*, **191**, 101–109.
- Villani, C. (2009) *Optimal Transport: Old and New*. Berlin: Springer-Verlag.
- Watomori, Y. and Jupp, P. E. (2005) Improved likelihood ratio and score tests on concentration parameters of von mises–fisher distributions. *Statistics & Probability Letters*, **72**, 93–102.
- Word, J. M., Lovell, S. C., LaBean, T. H., Taylor, H. C., Zalis, M. E., . . . , and Richardson, D. C. (1999) Visualizing and quantifying molecular goodness-of-fit: small-probe contact dots with explicit hydrogen atoms. *J. Mol. Biol.*, **285**, 1711–1733.

Appendix – Proofs

Proof of Proposition 1. First note that, for the squared Riemannian distance c used here, the a.e. uniqueness of the optimal transport plan is guaranteed by McCann (2001). Moreover, it follows from Section 2 in Gangbo and McCann (1996) that, since the cost function c belongs to the class of continuous mappings with domain $\mathcal{S}^{d-1} \times \mathcal{S}^{d-1}$, the support of the (unique) optimal transport plan $(\mathbf{I}_d \times \mathbf{F})\#\mathbf{P}^Z$ is c -cyclically monotone. Conversely, it directly follows from Theorem 1 in Beiglböck (2015) that a transport plan with c -cyclically monotone support is optimal. \square

Proof of Proposition 2. In view of Corollary 10 of McCann (2001), $\mathbf{F} = \exp_x(\nabla\psi(\mathbf{x}))$ is a bijection from \mathcal{S}^{d-1} to \mathcal{S}^{d-1} . Moreover, \mathbf{F} is continuous over \mathcal{S}^{d-1} according to Theorem 2.4 of Loeper (2011). Since \mathcal{S}^{d-1} equipped with d is a compact metric space, it follows (see e.g. Theorem 4.17 of Rudin (1976)) that \mathbf{F}^{-1} is continuous. The result follows. \square

Proof of Proposition 4. We first prove that, if the distribution of \mathbf{Z} is rotationally symmetric with location $\boldsymbol{\theta}_M$ and angular function f , then

$$F_f^*(\mathbf{Z}^\top \boldsymbol{\theta}_M) \boldsymbol{\theta}_M + \sqrt{1 - (F_f^*(\mathbf{Z}^\top \boldsymbol{\theta}_M))^2} \mathbf{S}_{\boldsymbol{\theta}_M}(\mathbf{Z}) \quad (.29)$$

is uniform over \mathcal{S}^{d-1} . Indeed, from the classical tangent-normal decomposition (see e.g. Paidaveine and Verdebout, 2017), we have that

$$\mathbf{Z} = (\mathbf{Z}^\top \boldsymbol{\theta}_M) \boldsymbol{\theta}_M + (1 - (\mathbf{Z}^\top \boldsymbol{\theta}_M)^2)^{1/2} \mathbf{S}_{\boldsymbol{\theta}_M}(\mathbf{Z})$$

is such that $\mathbf{S}_{\boldsymbol{\theta}_M}(\mathbf{Z})$ is uniformly distributed over $\mathcal{S}_{\boldsymbol{\theta}_M}^{p-2}$ and is independent of $\mathbf{Z}^\top \boldsymbol{\theta}_M$, which has distribution function F_f . It directly follows from the definition of F_f^* that $F_f^*(\mathbf{Z}^\top \boldsymbol{\theta}_M)$ has distribution function F_f^* , so that (.29) is uniform over \mathcal{S}^{d-1} . Now, to prove the c -cyclical monotonicity of the corresponding transport plan, it is enough show that, for any $\mathbf{z}_1, \mathbf{z}_2 \in \mathcal{S}^{d-1}$,

$$c(\mathbf{z}_1, \mathbf{F}(\mathbf{z}_1)) + c(\mathbf{z}_2, \mathbf{F}(\mathbf{z}_2)) \leq c(\mathbf{z}_2, \mathbf{F}(\mathbf{z}_1)) + c(\mathbf{z}_1, \mathbf{F}(\mathbf{z}_2)). \quad (.30)$$

Clearly, the optimal transport \mathbf{T} must satisfy $\mathbf{S}_{\boldsymbol{\theta}_M}(\mathbf{T}(\mathbf{z})) = \mathbf{S}_{\boldsymbol{\theta}_M}(\mathbf{z})$. Define the class

$$\mathcal{F} := \{\mathbf{T} \in \mathcal{S}(\mathbf{P}_{\boldsymbol{\theta}_M, f}, \mathbf{P}^U), \mathbf{S}_{\boldsymbol{\theta}_M}(\mathbf{T}(\mathbf{z})) = \mathbf{S}_{\boldsymbol{\theta}_M}(\mathbf{z})\}$$

of transport maps such that $\mathbf{S}_{\boldsymbol{\theta}_M}(\mathbf{T}(\mathbf{z})) = \mathbf{S}_{\boldsymbol{\theta}_M}(\mathbf{z})$. It readily follows from (3.17) that $\mathbf{F} \in \mathcal{F}$. Now, it remains to prove that \mathbf{F} is optimal within \mathcal{F} . Using again the equivalence between optimality and c -cyclical monotonicity, we only need to prove that (.30) holds for $\mathbf{z}_1, \mathbf{z}_2$ satisfying $\mathbf{S}_{\boldsymbol{\theta}_M}(\mathbf{z}_1) = \mathbf{S}_{\boldsymbol{\theta}_M}(\mathbf{z}_2)$. The problem is essentially equivalent to showing the c -cyclical monotonicity property of the transport on a unit circle with $\boldsymbol{\theta}_M$ as the origin. Without loss of generality, let us assume that $d(\mathbf{z}_1, \boldsymbol{\theta}_M) < d(\mathbf{z}_2, \boldsymbol{\theta}_M)$ and $d(\mathbf{z}_2, \boldsymbol{\theta}_M) < d(\mathbf{F}(\mathbf{z}_1), \boldsymbol{\theta}_M)$. Let

$$\alpha_1 := d(\mathbf{z}_1, \mathbf{z}_2), \quad \alpha_2 := d(\mathbf{z}_2, \mathbf{F}(\mathbf{z}_1)), \quad \text{and} \quad \alpha_3 := d(\mathbf{F}(\mathbf{z}_1), \mathbf{F}(\mathbf{z}_2)).$$

Since, in view of (3.17), $\mathbf{z}_1^\top \boldsymbol{\theta} > \mathbf{z}_2^\top \boldsymbol{\theta}$ implies $\mathbf{F}^\top(\mathbf{z}_1) \boldsymbol{\theta}_M > \mathbf{F}^\top(\mathbf{z}_2) \boldsymbol{\theta}_M$, we have that

$$d(\mathbf{z}_1, \mathbf{F}(\mathbf{z}_2)) = \alpha_1 + \alpha_2 + \alpha_3.$$

The problem thus reduces to proving that

$$(\alpha_1 + \alpha_2)^2 + (\alpha_2 + \alpha_3)^2 \leq (\alpha_1 + \alpha_2 + \alpha_3)^2 + \alpha_2^2,$$

which obviously holds true. \square

Proof of Proposition 5. In the population version, the transport map \mathbf{F} induces the transport plan

$$\gamma := (\mathbf{I}_d \times \mathbf{F})\#P^{\mathbf{Z}} \in \Gamma(P^{\mathbf{Z}}, P^{\mathbf{U}}) \quad (.31)$$

with marginals $P^{\mathbf{Z}}$ and $P^{\mathbf{U}}$ and support the graph $\{(\mathbf{z}, \mathbf{F}(\mathbf{z})) \mid \mathbf{z} \in \mathcal{S}^{d-1}\}$ of \mathbf{F} . Its sample version $\mathbf{F}^{(n)}$ similarly induces the transport plan

$$\gamma^{(n)} := (\mathbf{I}_d \times \mathbf{F}^{(n)})\#P^{(n)} \in \Gamma(P^{(n)}, P_{\mathbf{U}}^{(n)}), \quad (.32)$$

with marginals the empirical distribution $P^{(n)}$ of the sample $\mathbf{Z}_1, \dots, \mathbf{Z}_n$ and the uniform distribution $P_{\mathbf{U}}^{(n)}$ over the grid $\mathbb{G}^{(n)}$; $\gamma^{(n)}$ is supported on the (discrete) graph $\{(\mathbf{Z}_i^{(n)}, \mathbf{F}^{(n)}(\mathbf{Z}_i^{(n)})) \mid i = 1, \dots, n\}$ of $\mathbf{F}^{(n)}$. The proof is based on two lemmas.

Lemma 11 *Let $\gamma^{(n)}$ and γ as defined in (.31) and (.32). We have that $\gamma^{(n)}$ converges weakly to γ as $n \rightarrow \infty$.*

Proof of Lemma 11. By construction, $\gamma^{(n)}$, with marginals $P^{(n)}$ and $P_{\mathbf{U}}^{(n)}$, has c -cyclically monotone support. Since $P^{(n)}$ converges weakly to $P^{\mathbf{Z}}$ and $P_{\mathbf{U}}^{(n)}$ has uniformly bounded support, $\gamma^{(n)}$ is tight. Hence, by the Prohorov Theorem, there exist subsequences $\gamma^{(n_k)}$ converging weakly to some probability measure γ^∞ , say, where $\gamma^\infty \in \Gamma(P^{\mathbf{Z}}, P^{\mathbf{U}})$. For all n_k , $\gamma^{(n_k)}$ has c -cyclically monotone support. It thus follows from Villani (2009, pages 64-65) that the support of γ^∞ also is c -cyclically monotone and therefore coincides with the unique optimal transport plan of Proposition 1, which is γ . Assume that $\gamma^{(n)}$ does not converge weakly to γ . Then, either (a) there exists no weakly convergent subsequence, or (b) there exists a subsequence $\gamma^{(n_k)}$ converging to $\gamma^\infty \neq \gamma$. Because of tightness, (a) is impossible; (b) is impossible as well in view of the c -cyclical monotonicity argument above; the claim follows. \square

Now, Proposition 1 entails that

$$\mathbf{F}(\mathbf{x}) = \exp_{\mathbf{x}}(-\nabla\psi(\mathbf{x})),$$

where (see (2) in Loeper (2009)) the c -concave optimal potential ψ and its c -transform ϕ are such that

$$\psi(\mathbf{x}) + \phi(\mathbf{F}(\mathbf{x})) = c(\mathbf{x}, \mathbf{F}(\mathbf{x})).$$

For a c -concave function g , define the c -superdifferential of g as

$$\partial g := \left\{ (\mathbf{x}, \mathbf{y}) \in \mathcal{S}^{d-1} \times \mathcal{S}^{d-1} \mid g(\mathbf{z}) \leq g(\mathbf{x}) + c(\mathbf{z}, \mathbf{y}) - c(\mathbf{x}, \mathbf{y}) \text{ for all } \mathbf{z} \in \mathcal{S}^{d-1} \right\}.$$

Write $\partial g(\mathbf{x})$ for the set of points $\mathbf{y} \in \mathcal{S}^{d-1}$ such that $(\mathbf{x}, \mathbf{y}) \in \partial g$. Since \mathbf{F} is a.s. unique, we have that

$$\mathbf{F}(\mathbf{x}) = \exp_{\mathbf{x}}(-\nabla\psi(\mathbf{x})) = \partial\psi(\mathbf{x})$$

is a singleton. Writing $\text{Supp}(P)$ for the support of a probability measure P , it follows from Section 2 in [Gangbo and McCann \(1996\)](#) that the c -superdifferential of the optimal potential ψ is such that $\text{Supp}(\gamma) \subset \partial\psi$.

A potential $\psi^{(n)}$ such that $\mathbf{F}^{(n)} = \exp(-\nabla\psi^{(n)})$ similarly is associated with $\mathbf{F}^{(n)}$ (see, e.g., Theorem 5.10 (ii) in [Villani \(2009\)](#)). The next lemma establishes the convergence of $\partial\psi^{(n)}$ to $\partial\psi$ in the Painlevé-Kuratowski sense. Recall that the sequence $\partial g^{(n)}$ of c -superdifferentials converges to ∂g in the Painlevé-Kuratowski sense (notation: $\partial g^{(n)} \rightarrow_{\text{PK}} \partial g$) if (i) the *outer limit set* $\limsup_{n \rightarrow \infty} \partial g^{(n)}$ —namely, the set of points $(\mathbf{x}, \gamma) \in \mathcal{S}^{d-1} \times \mathcal{S}^{d-1}$ for which there exists a sequence $(\mathbf{x}_n, \gamma_n) \in \partial g^{(n)}$ admitting a subsequence converging to (\mathbf{x}, γ) —and (ii) the *inner limit set* $\liminf_{n \rightarrow \infty} \partial g^{(n)}$ —the set of points $(\mathbf{x}, \gamma) \in \mathcal{S}^{d-1} \times \mathcal{S}^{d-1}$ which are limits of sequences $(\mathbf{x}_n, \gamma_n) \in \partial g^{(n)}$ —coincide with ∂g .

Lemma 12 *Denoting by $\partial\psi^{(n)}$ and $\partial\psi$ the c -subdifferentials of the empirical and population potential $\psi^{(n)}$ and ψ , respectively, we have that $\partial\psi^{(n)} \rightarrow_{\text{PK}} \partial\psi$ as $n \rightarrow \infty$.*

Proof of Lemma 12. Fix $\mathbf{z}_0 \in \mathcal{S}^{d-1}$. In view of Proposition 2, $\mathbf{z} \mapsto \mathbf{F}(\mathbf{z})$ is continuous at \mathbf{z}_0 . Therefore, denoting by $C_\delta(\mathbf{z})$ the hyperspherical cap obtained as the intersection between \mathcal{S}^{d-1} and the ball $B_\delta(\mathbf{z})$ with radius δ centered at \mathbf{z} , for each $\epsilon > 0$, there exists a $\delta = \delta(\epsilon) > 0$ such that for all \mathbf{z} with $c(\mathbf{z}, \mathbf{z}_0) < \delta$, $\mathbf{F}(\mathbf{z}) = \partial\psi(\mathbf{z}) \subset C_\epsilon(\mathbf{F}(\mathbf{z}_0))$. Since $\text{Supp}(\gamma) \subset \partial\psi$, we have that

$$\gamma(B_\delta(\mathbf{z}_0) \times C_\epsilon(\mathbf{F}(\mathbf{z}_0))) = \gamma(B_\delta(\mathbf{z}_0) \times \mathcal{S}^{d-1}) = \mathbf{P}^{\mathbf{Z}}(B_\delta(\mathbf{z}_0)) =: \eta > 0.$$

Taking a decreasing sequence $\epsilon_k \downarrow 0$ and the corresponding sequence $\delta_k = \delta(\epsilon_k) \downarrow 0$, we therefore have that

$$\gamma(B_{\delta_k}(\mathbf{z}_0) \times C_{\epsilon_k}(\mathbf{F}(\mathbf{z}_0))) = \mathbf{P}^{\mathbf{Z}}(B_{\delta_k}(\mathbf{z}_0)) =: \eta_k > 0.$$

Now, Lemma 11 entails that there exists N_k such that for $n > N_k$,

$$\gamma^{(n)}(B_{\delta_k}(\mathbf{z}_0) \times C_{\epsilon_k}(\mathbf{F}(\mathbf{z}_0))) \geq \eta_k/2.$$

Therefore, since $\text{Supp}(\gamma^{(n)}) \subset \partial\psi^{(n)}$, there exists a sequence

$$(\mathbf{x}_{n_k}, \gamma_{n_k}) \in \partial\psi^{(n)} \cap (B_{\delta_k}(\mathbf{z}_0) \times C_{\epsilon_k}(\mathbf{F}(\mathbf{z}_0)))$$

converging as $k \rightarrow \infty$ to $(\mathbf{z}_0, \mathbf{F}(\mathbf{z}_0))$. This entails that (i) $\partial\psi^{(n)}$ does not escape to the horizon in the sense of [del Barrio et al. \(2021\)](#) and (ii) we can extract a subsequence of $\partial\psi^{(n)}$ (which are c -cyclically monotone sets) converging to $(\mathbf{z}_0, \mathbf{F}(\mathbf{z}_0))$ for any arbitrarily fixed $\mathbf{z}_0 \in \mathcal{S}^{d-1}$. The Painlevé-Kuratowski convergence then follows from Lemma 2.9 and Theorem 2.8 in [del Barrio et al. \(2021\)](#). \square

To conclude with the proof of Proposition 5, assume that there exists a sequence $(\mathbf{x}_n, \gamma_n) \in \mathcal{S}^{d-1} \times \partial\psi^{(n)}(\mathbf{x}_n)$ such that for all n

$$c(\gamma_n, \partial\psi(\mathbf{x}_n)) > 0. \tag{.33}$$

Since \mathcal{S}^{d-1} is compact, there exists a subsequence of \mathbf{x}_n that converges to some $\mathbf{x} \in \mathcal{S}^{d-1}$. The continuity of $\mathbf{z} \mapsto \mathbf{F}(\mathbf{z}) = \partial\psi(\mathbf{z})$ together with Lemma 12 (which entails that γ_n converges to $\partial\psi(\mathbf{x}) = \mathbf{F}(\mathbf{x})$) contradict (.33). The result follows. \square

Proof of Proposition 6. Assume that $n_0 = 0$ or 1 . First note that an element $\mathbb{G}_{ij}^{(n)}(\widehat{\boldsymbol{\theta}}^{(n)})$ of $\mathbb{G}_{ij}^{(n)}(\widehat{\boldsymbol{\theta}}^{(n)})$ decomposes into

$$\begin{aligned} \mathbb{G}_{ij}^{(n)}(\widehat{\boldsymbol{\theta}}^{(n)}) &= \left((\mathbb{G}_{ij}^{(n)}(\widehat{\boldsymbol{\theta}}^{(n)}))^{\top} \widehat{\boldsymbol{\theta}}^{(n)} \right) \widehat{\boldsymbol{\theta}}^{(n)} + \left(\mathbf{I}_p - \widehat{\boldsymbol{\theta}}^{(n)} (\widehat{\boldsymbol{\theta}}^{(n)})^{\top} \right) \mathbb{G}_{ij}^{(n)}(\widehat{\boldsymbol{\theta}}^{(n)}) \\ &= Q_* \left(1 - \frac{i}{n_R + 1} \right) \widehat{\boldsymbol{\theta}}^{(n)} + \left(1 - Q_*^2 \left(1 - \frac{i}{n_R + 1} \right) \right)^{1/2} \boldsymbol{\Gamma}_{\widehat{\boldsymbol{\theta}}^{(n)}} \mathbf{s}_j \end{aligned} \quad (.34)$$

Therefore, since $\widehat{\boldsymbol{\theta}}^{(n)}$ is $\mathbf{Z}_{(\cdot)}^{(n)}$ -measurable, we have that, conditionally on $\mathbf{Z}_{(\cdot)}^{(n)}$, the n -tuple of vectors

$$\mathbf{F}^{(n)}(\mathbf{Z}^{(n)}) = (\mathbf{F}^{(n)}(\mathbf{Z}_1^{(n)}), \dots, \mathbf{F}^{(n)}(\mathbf{Z}_n^{(n)}))$$

is uniform over the $n!$ permutations of the n gridpoints—irrespective of the value of $\mathbf{Z}_{(\cdot)}^{(n)}$; therefore, $\mathbf{F}^{(n)}(\mathbf{Z}^{(n)})$ is also unconditionally uniform over these permutations. If $n_0 > 1$, the situation is exactly the same, except that the $n_0!$ permutations involving the n_0 copies of $\widehat{\boldsymbol{\theta}}^{(n)}$ are undistinguishable so that the $n!$ permutations reduce to $n!/n_0!$ permutations with repetitions. This, however, can be avoided by breaking the n_0 ties at the origin as in Hallin et al. (2021a). Point (ii) follows. Points (iii), (iv), and (v) are direct consequences of (.34) and the fact that the uniform over the grid $\mathbb{G}^{(n)}$ factorizes into the product of uniform measures over the two grids involved in its construction (step (2a)). \square

Proof of Proposition 7. Points (i) and (ii) follow exactly along the same lines as in the proof of Proposition 6. We therefore focus on point (iii) assuming that the grid does not exhibit any multiplicity at $\widehat{\boldsymbol{\theta}}^{(n)}$ (either $n_0 = 0$ or 1 , or the tie-breaking device has been performed). In view of Basu (1959) (see Proposition E.4 in Appendix E of Hallin et al. (2021a)), since $\mathbf{Z}_{(\cdot)}^{(n)}$ is sufficient and complete, we only have to show that the sigma-field $\sigma(\mathbf{Z}_{(\cdot)}^{(n)}, \mathbf{R}^{(n)}, \mathbf{S}^{(n)})$ is essentially equivalent to the Borel σ -field \mathcal{B}^{d-1} . Since $\widehat{\boldsymbol{\theta}}^{(n)}$ is $\mathbf{Z}_{(\cdot)}^{(n)}$ -measurable and in view of (.34), the mapping $\mathbf{z} \in \mathcal{S}^{d-1} \mapsto (\mathbf{z}_{(\cdot)}, \mathbf{R}(\mathbf{z}), \mathbf{S}(\mathbf{z}))$ clearly is injective. The claim follows. \square

Proof of Proposition 8. Since the Riemannian distance is invariant under orthogonal transformations, it holds that $c(\mathbf{z}_i^{(n)}, \mathbb{G}_j^{(n)}) = c(\mathbf{Oz}_i^{(n)}, \mathbf{O}\mathbb{G}_j^{(n)})$ for all $i, j \in \dots$ and all orthogonal matrix \mathbf{O} . It follows that the empirical optimal transport pushing $n^{-1} \sum_{i=1}^n \delta(\mathbf{z}_i^{(n)})$ forward to $n^{-1} \sum_{i=1}^n \delta(\mathbb{G}_i^{(n)})$ (where $\delta(\mathbf{z})$ is the Dirac distribution at \mathbf{z}) and the empirical optimal transport pushing $n^{-1} \sum_{i=1}^n \delta(\mathbf{Oz}_i^{(n)})$ forward to $n^{-1} \sum_{i=1}^n \delta(\mathbf{O}\mathbb{G}_i^{(n)})$ coincide up to the orthogonal transformation \mathbf{O} , that is, if $\mathbf{F}_{\mathbf{z}}^{(n)}(\mathbf{z}_i) = \mathbb{G}_j^{(n)}$, then $\mathbf{F}_{\mathbf{Oz}}^{(n)}(\mathbf{Oz}_i) = \mathbf{O}\mathbb{G}_j^{(n)}$. Point (i) of the proposition follows. Point (ii) is a straightforward corollary to Point (i). \square

Proof of Proposition 9. Let $\mathbf{Z}_1^{(n)}, \dots, \mathbf{Z}_n^{(n)}$ be i.i.d. with directional distribution function \mathbf{F} . Since $\mathbf{F}^{(n)}(\mathbf{Z}_i^{(n)})$ and $\mathbf{F}_0(\mathbf{Z}_i^{(n)})$ are unit vectors,

$$T_n = n^{-1} \sum_{i=1}^n \|\mathbf{F}^{(n)}(\mathbf{Z}_i^{(n)}) - \mathbf{F}_0(\mathbf{Z}_i^{(n)})\|^2 = 2 \left(1 - n^{-1} \sum_{i=1}^n (\mathbf{F}^{(n)}(\mathbf{Z}_i^{(n)}))^{\top} \mathbf{F}_0(\mathbf{Z}_i^{(n)}) \right).$$

Therefore, we just need to study the asymptotic behavior of

$$W_n := n^{-1} \sum_{i=1}^n (\mathbf{F}^{(n)}(\mathbf{Z}_i^{(n)}))^{\top} \mathbf{F}_0(\mathbf{Z}_i^{(n)}).$$

We readily have that

$$\begin{aligned}
W_n &= n^{-1} \sum_{i=1}^n (\mathbf{F}^{(n)}(\mathbf{Z}_i^{(n)}))^\top \mathbf{F}_0(\mathbf{Z}_i^{(n)}) \\
&= n^{-1} \sum_{i=1}^n (\mathbf{F}^{(n)}(\mathbf{Z}_i^{(n)}) - \mathbf{F}(\mathbf{Z}_i^{(n)}))^\top \mathbf{F}_0(\mathbf{Z}_i^{(n)}) + n^{-1} \sum_{i=1}^n (\mathbf{F}(\mathbf{Z}_i^{(n)}))^\top \mathbf{F}_0(\mathbf{Z}_i^{(n)}) \\
&=: W_{1n} + W_{2n}, \text{ say.}
\end{aligned}$$

The Cauchy-Schwartz inequality and Proposition 5 jointly entail that

$$\begin{aligned}
|W_{1n}| &\leq n^{-1} \sum_{i=1}^n |(\mathbf{F}^{(n)}(\mathbf{Z}_i^{(n)}) - \mathbf{F}(\mathbf{Z}_i^{(n)}))^\top \mathbf{F}_0(\mathbf{Z}_i^{(n)})| \\
&\leq n^{-1} \sum_{i=1}^n \|\mathbf{F}_0(\mathbf{Z}_i^{(n)})\| \|\mathbf{F}^{(n)}(\mathbf{Z}_i^{(n)}) - \mathbf{F}(\mathbf{Z}_i^{(n)})\| \\
&= n^{-1} \sum_{i=1}^n \|\mathbf{F}^{(n)}(\mathbf{Z}_i^{(n)}) - \mathbf{F}(\mathbf{Z}_i^{(n)})\| \\
&\leq \max_{1 \leq i \leq n} \|\mathbf{F}^{(n)}(\mathbf{Z}_i^{(n)}) - \mathbf{F}(\mathbf{Z}_i^{(n)})\|,
\end{aligned}$$

which is $o_p(1)$ as $n \rightarrow \infty$. Now, if $\mathbf{F} = \mathbf{F}_0$, we have that $W_{2n} = 1$ almost surely so that W_n converges to one in probability. As a result, T_n converges to zero in probability when $\mathbf{F} = \mathbf{F}_0$. When $\mathbf{F} \neq \mathbf{F}_0$, the law of large numbers entails that W_{2n} converges in probability to $E[(\mathbf{F}(\mathbf{Z}_1^{(n)}))^\top \mathbf{F}_0(\mathbf{Z}_1^{(n)})] < 1$. The result follows. \square

Proof of Proposition 10. In this proof, we write \mathbf{F}_ℓ for $\mathbf{F}(\mathbf{Y}_\ell^{(n)})$ and $\mathbf{F}_\ell^{(n)}$ for $\mathbf{F}^{(n)}(\mathbf{Y}_\ell^{(n)})$. Since $\sum_{\ell=1}^n (a_{i\ell}^{(n)} - \bar{a}_i^{(n)}) = 0$,

$$\sum_{\ell=1}^n (a_{i\ell}^{(n)} - \bar{a}_i^{(n)})^2 = - \sum_{j \neq \ell} (a_{ij}^{(n)} - \bar{a}_i^{(n)}) (a_{i\ell}^{(n)} - \bar{a}_i^{(n)}).$$

Letting $\Gamma_{i;\mathbf{J}}^{(n_i)} := n^{-1/2} \sum_{\ell=1}^n (a_{i\ell}^{(n)} - \bar{a}_i^{(n)}) \mathbf{J}(\mathbf{F}_\ell)$ and $\boldsymbol{\gamma}_\ell^{(n)} := \mathbf{J}(\mathbf{F}_\ell^{(n)}) - \mathbf{J}(\mathbf{F}_\ell)$, we have that

$$\begin{aligned}
E[\|\Delta_{i;\mathbf{J}}^{(n_i)} - \Gamma_{i;\mathbf{J}}^{(n_i)}\|^2] &= n^{-1} \sum_{j, \ell=1}^n (a_{ij}^{(n)} - \bar{a}_i^{(n)}) (a_{i\ell}^{(n)} - \bar{a}_i^{(n)}) E[(\boldsymbol{\gamma}_j^{(n)})' \boldsymbol{\gamma}_\ell^{(n)}] \\
&= n^{-1} \sum_{\ell=1}^n (a_{i\ell}^{(n)} - \bar{a}_i^{(n)})^2 (E[\|\boldsymbol{\gamma}_1^{(n)}\|^2] - E[(\boldsymbol{\gamma}_1^{(n)})' \boldsymbol{\gamma}_2^{(n)}]) \\
&\leq 2E[\|\boldsymbol{\gamma}_1^{(n)}\|^2].
\end{aligned}$$

It follows from the continuity of \mathbf{J} and Proposition 5 that $\boldsymbol{\gamma}_1^{(n)}$ converges to 0 a.s. Since $E\|\mathbf{J}(\mathbf{F}_1^{(n)})\|^2 \rightarrow E\|\mathbf{J}(\mathbf{F}_1)\|^2 < \infty$ as $n \rightarrow \infty$, $E\|\boldsymbol{\gamma}_1^{(n)}\|^2 = o(1)$ as $n \rightarrow \infty$ (see, e.g., Theorem 5.5 in Chapter 3 of [Shorack \(2000\)](#)). As a result,

$$\mathbf{Q}_J^{(n)} = \Gamma_J^{(n)'} (\mathbf{I}_m \otimes \mathbf{D}_J^{-1}) \Gamma_J^{(n)} + o_p(1)$$

as $n \rightarrow \infty$, where $\Gamma_J^{(n)} := (\Gamma_{1;\mathbf{J}}^{(n_1)'}, \dots, \Gamma_{m;\mathbf{J}}^{(n_m)'})'$. It follows immediately from the Central Limit Theorem that $\Gamma_J^{(n)}$ is asymptotically normal with mean zero and covariance $(\mathbf{I}_m - \mathbf{C}_m) \otimes \mathbf{D}_J$, where $\mathbf{C}_m = (r_i^{1/2} r_j^{1/2})_{1 \leq i, j \leq m} = \mathbf{v}_m \mathbf{v}_m'$

with $\mathbf{v}_m := (r_1^{1/2}, \dots, r_m^{1/2})'$. Note that \mathbf{C}_m is idempotent, since

$$\mathbf{C}_m^2 = \mathbf{v}_m \mathbf{v}_m' \mathbf{v}_m \mathbf{v}_m' = \mathbf{v}_m \left(\sum_{j=1}^m r_j \right) \mathbf{v}_m' = \mathbf{v}_m \mathbf{v}_m' = \mathbf{C}_m.$$

The result then follows from noticing that $(\mathbf{I}_m \otimes \mathbf{D}_J^-)[(\mathbf{I}_m - \mathbf{C}_m) \otimes \mathbf{D}_J]$ is idempotent with trace $(m-1)d^*$. \square